Am Zentrum für Integrative Neurowissenschaften der Universität Tübingen und der Neurologischen Universitätsklinik Tübingen, Abteilung Neurologie mit Schwerpunkt Neurodegenerative Erkrankungen

'Elucidating projection patterns and postsynaptic partners of medial paracapsular intercalated cells in the mouse amygdala'

Inaugural-Dissertation
zur
Erlangung des Doktorgrades der Medizin
der Medizinischen Fakultät
der Eberhard Karls Universität
zu Tübingen

vorgelegt von

Gärtner, Anna

2017

Dekan: Prof. Dr. I. B. Autenrieth

1. Berichterstatter: Professor Dr. Th. Gasser

2. Berichterstatter: Professor Dr. C. Schwarz

Tag der Disputation: 27.07.2017

’(...) die ganze Wirklichkeit des Wissens projektiert sich in der Angst als ungeheures Nichts der Unwissenheit.’

Kirkegaard Sören in *Der Begriff Angst*

“Hast du Angst?”, fragt Remi (...).
“Nein. Ich habe keine Angst ... Höchstens ein kleines bisschen”

Chatelet Noelle in *Das Sonnenblumenmädchen*

Contents

Nomenclature

AL	Ansa lenticularis
r	correlation coefficent
r square	coefficent of determination
Astr-p	Astr-projecting
Astr	amygdalo-striatal transition zone
BA	basal amygdala
CEA	central nucleus of the amygdala
BLA-p	BLA-projecting
BLA	basolateral amygdala
CEA-p	CEA-projecting
CeC	capsular subnucleus of the central amygdala
CeL	lateral subnucleus of the central amygdala
CeM	medial subnucleus of the central amygdala
ChAT	cholin acetyl transferase
CP	caudate putamen
Cp	central-projecting
CRH	corticotropin releasing hormone
CS	conditioned stimulus
Cy3	Cyan 3
Cy5	Cyan 5
DAB	diaminobenzidine
EC	external capsule

GABA	gamma-aminobutric acid
GFP	Green Fluorescent Protein
GP	Globus pallidus
IC	internal capsule
IL	infra limbic cortex
IMC-p	IMC-projecting
IMC	intermediate capsule
IN	interneuron
IPAC	posterior limb of the anterior commissure
ITC	intercalated cell
L-ITC	large ITC
LA	lateral amygdala
lpITC	lateral paracapsular ITC
MCp	medial capsula- projecting
MEA	medial extended amygdala
mGluR	metabotropic glutamate receptor
mITC	ITC main cluster
mm	millimeter
mPFC	medial prefrontal cortex
mpITC	medial paracapsular intercalated cell
NK-1	Neurokinin-1
nm	nanometer
OWA	one way anova
PAG	periaqueductal grey
PBS	phosphate buffered saline

PKC	proteinkinase C
PL	prelimbic cortex
PN	principal neuron
PTSD	posttraumatic stress disorder
RT	room temperature
SEM	standard error of the mean
SLp	sublenticular-projecting
SOM	somatostatine
US	unconditioned stimulus
VTA	ventral tegmental area

1 Introduction

1.1 Role of the amygdala in fear behavior

The amygdala is a key brain structure implicated in emotional processing (Davis & Shi, 2000; LeDoux, 2000). Its role is at the interface of rapidly encoding valence associated with environmental stimuli and the coordination of the organism's adapted behavioral response (Adolphs, 2013). Additionally, it participates in several mood-related behaviors such as reward, attention and even food seeking, but is best known and investigated function is that of its relation to processing of and responding to fear (Janak & Tye, 2015). This requires adapting the behavior to avoid threatening stimuli (Adolphs, 2013). The processing between incoming threatening stimuli and the resulting fearful behavior is what Adolphs calls fear (Adolphs, 2013). This process needs to be adapted to learn from past and current situations. This adaptation serves as an evolutionary important survival kit, but can cause severe suffering if it then pathologically leads to excessive behavioral responses in prevalent mental illnesses like anxiety disorders or post traumatic stress disorder (PTSD) (Jovanovic & Norrholm, 2011; Milad et al., 2013). In laboratories, fear behavior is mainly investigated using Pavlovian fear conditioning and fear extinction (Pape & Pare, 2010). In fear conditioning, an initially neutral stimulus, the conditioned stimulus (CS), is paired several times with a threatening stimulus, the unconditioned stimulus (US). So the CS is associated with the US and is then alone able to induce fearful behavior. In extinction training the CS is presented many times alone and is thus learned to be uncoupled from the US so that it does not evoke fear behavior anymore (Maren, 2001). Extinction learning has a clinical relevance, as it is the basis for cognitive behavioral therapy (Keane et al., 2006), a treatment applied to people suffering from pathological fear (Milad et al., 2013). Several lines of evidence show that the amygdala plays a key role not only in the expression of fear, but also in the acquisition and storage of fear and extinction memory (Maren, 2003; Sigurdsson et al., 2007; Pape & Pare, 2010). Its involvement in fear processing is seen throughout vertebrate species including rodents, guinea pigs cats, monkeys and humans (Weiskrantz, 1956; Phelps & LeDoux, 2005; Adolphs, 2013), which makes the mouse model an ideal medium for investigation. In summary, the amygdala is a brain structure involved in emotional processing, and in adapting physiological as well as pathological fear behavior to threatening stimuli. To further understand its relevance in fear behavior and manipulations that can serve as treatments of anxiety disorders, the identification of the underlying neuroanatomical background is important.

1.2 Functional anatomy of the amygdala and closely related nuclei

The amygdala is a brain structure of the limbic system situated deep in the temporal lobe, located within the fiber bundles of the external capsule (EC), the intermediate capsule (IMC) and the internal capsule (IC) (Pape & Pare, 2010). Its structure, as well as its main connectivity is highly preserved in vertebrates (Price, 2003; Janak & Tye, 2015). The amygdala consists of a heterogeneous group of nuclei distinguishable due to their cytoarchitectonic structure, immunohistochemical markers and connectivity (Pitkänen et al., 1997; LeDoux, 2007). (1) The basolateral group consists of the lateral (LA), the basal (BA) nucleus, together referred as BLA, and the accessory basal nucleus. (2) The cortical group consists of the cortical nuclei and the nucleus of the olfactory tract (Pitkänen et al., 1997). (3) The centromedial group consists of the central nucleus (CEA) and the medial extended amygdala (MEA). The CEA can be further subdivided in a medial (CeM), capsular (CeC), and lateral (CeL) sub nucleus (Cassell et al., 1999). (4) The intercalated cells (ITCs) are dense cell clusters located within and along the fiber bundles surrounding the BLA (Millhouse, 1986). In the following I refer, if not otherwise stated, to the rodent amygdala. The main flow of information related to fear through the amygdala includes the BLA as main sensory input site, distributing received information directly or via ITCs to the CEA, as main output nuclei with downstream projections (Pape & Pare, 2010; Duvarci & Pare, 2014). Further parallel or additional pathways have been described, but remain to be elucidated in their full extend. In the following, I will focus on the main input and output nuclei of the amygdala - the BLA and the CEA, on parts of the extended amygdala, the MEA and closely related neighboring nuclei, the amygdalostriatal transition zone (Astr) and the interstitial nucleus of the posterior limb of the anterior commissure (IPAC), and as well on ITCs (Fig. 1).

BLA. The BLA, situated lateral of the intermediate capsule, has cortex-like cellular compositions without being organized in the typical separate layers. The LA and BA contain 80-85% glutamatergic principal neurons (PN) and 15-20% local GABAergic interneurons (IN), belonging to different morphologically, molecularly and functionally defined classes. The BLA is reciprocally connected to different thalamic nuclei and higher order sensory or limbic association cortices, including the medial prefrontal cortex (mPFC) (Pape & Pare, 2010). The LA provides feed forward activation directly to the CeL and feed forward inhibition through ITCs. The BA projects directly to the CeM (Duvarci & Pare, 2014). Functionally, sensory information, i.e. about CS and US in fear conditioning, reaches the amygdala mainly via sensory afferences to the LA. Several lines of evidence show that fear learning takes place in this subdivision of the BLA (Pape & Pare, 2010; Duvarci & Pare, 2014). The BA is crucially

involved in extinction learning and extinction retrieval. It receives input from the infra limbic region (IL) of the mPFC. This region is associated with extinction learning and memory. The BA is also involved in fear learning, receiving input additionally from the prelimbic cortex (PL), the mPFC region associated with fear learning. Different types of BA cells were shown to be active during fear or extinction training and the correlating behavioral fear state (Herry et al., 2008; Duvarci & Pare, 2014; Senn et al., 2014).

CEA. The CEA is located medial to the IMC. It is thought to be a ventral extension of the striatum, as it mainly consists of spiny GABAergic neurons. It receives a major input from BLA and ITCs (Duvarci & Pare, 2014). Furthermore, CEA cells are connected among themselves, intra- and intersubdivisionally (Ciocchi et al., 2010; Haubensak et al., 2010; Li et al., 2013). It is seen as the main output site of the amygdaloid complex to dopaminergic midbrain and brainstem regions like the ventral tegmental area (VTA) and the periaqueductal gray (PAG) (Pape & Pare, 2010). Recent evidence suggests that the CEA is not only the passive output relay of the amygdala, but participates in acquisition and storage of fear memory (Wilensky et al., 2006; Li et al., 2013).

CeM. The medial sub nucleus is under tonic inhibition, mainly by CeL neurons (Ciocchi et al., 2010) and receives input from the ITC main cluster (mITC) (Blaesse et al., 2015). It projects to brainstem regions initiating motor-, endocinologic-, and autonomous nervous system related behavioral responses (LeDoux et al., 1988). It is known to be crucial for the expression of fear (Ciocchi et al., 2010) (Fig. 1).

CeC/CeL. Although sub nuclei are distinguished in anatomical studies (Cassell et al., 1999), their functional specialization or differences in fear processing are poorly reported. Little is known about the capsular sub nucleus. In the lateral sub nucleus, three major subpopulations of cells were found: cells expressing proteinkinase Cδ (PKC δ), somatostatine (SOM), and corticotropin releasing hormone (CRH). The following, if not stated differently, will only refer to the first two populations. These two are known to differ in morphological and functional aspects. Approximately half of CeL cells express PKC δ and are mainly SOM-negative (SOM^-) labeled. The second major proportion of CeL cells is SOM-positive (SOM^+) and analog mainly PKC δ-negative (PKC δ^-) (Ciocchi et al., 2010; Haubensak et al., 2010; Li et al., 2013). CRH-positive (CRH^+) cells are non-overlapping with PKC δ^+-positive (PKC δ^+) cells (Haubensak et al., 2010). Regarding their connectivity, the SOM^+ population receives input from the LA (Li et al., 2013). The CeL also receives input from medial paracapsular ITCs (mpITCs) (Duvarci & Pare, 2014), but it still remains to be elucidated, which of the two populations in CeL is targeted. Reciprocal connection exists between SOM^+ and

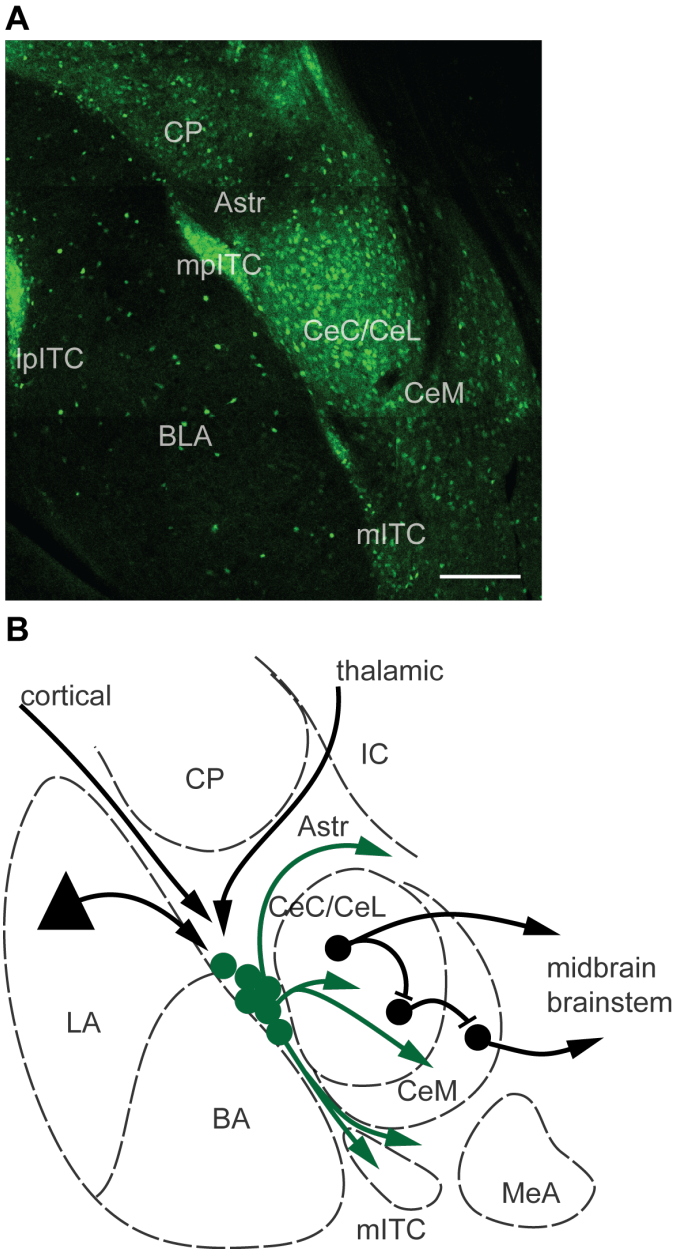

Figure 1: **Known connectivity of mpITCs**
(A) Fluorescent coronal brain slice of a GAD67-GFP mouse showing the anatomical organization of the amygdala with the BLA as part of the basolateral group, the CEA with CeC/CeL and CeM as part of the centromedial group and lpITC, mITC, and mpITC cluster of the ITC cluster formation. Further depicted are the adjacent Astr and the CP. As the BLA consists mainly of glutamatergic neurons GFP-labeling is scarce there. On the contrary the richness of GABAergic neurons in the CEA and the ITC cluster corresponds to the dense GFP-labeling there. Scale bar: 200 μm. (B) Simplified scheme of mpITC known connectivity in the amygdala fear circuit : Shown is sensory input from cortical and thalamic regions and the BLA and outgoing projections to the mITCs, the Astr, and the CEA. In the CEA fear related information is further processed from ($Fear_{ON}$) cells directly to midbrain areas or via ($Fear_{OFF}$) cells to CeM to brainstem areas, eliciting fear behavior. $Fear_{ON}$ cells are suggested to bee the SOM^{-}, mainly the PKC δ^{+} cell population in CeL (adapt. f. Asede et al., 2015; Duvarci & Pare, 2014; Busti et al., 2011).

PKC δ^+ cells (Ciocchi et al., 2010; Haubensak et al., 2010). CeL output consists of tonic inhibition of CeM neurons which is mainly made by SOM$^-$ cells (Li et al., 2013). A proportion of SOM$^+$ cells sends long range projections to the VTA and the PAG (Penzo et al., 2015). Functionally, PKC δ^+ cells (i.e. SOM$^-$ cells) are thought to correspond to so called Fear_{OFF} cells as their silencing increases the fear response via disinhibition of CeM cells (Ciocchi et al., 2010; Haubensak et al., 2010). SOM$^+$ cells (i.e. PKC δ^- cells) are so called Fear_{ON} cells, as they can control the fear response directly via long range projections or by disinhibiting Fear_{OFF} cells (Li et al., 2013; Penzo et al., 2014, 2015). Recent results show that activation of SOM$^+$ cells even triggers unconditioned fear expression (Penzo et al., 2015).

MEA. The MEA is located mediodorsally to the IMC. Morphological, it is similar to the CEA and thus striatal-like (McDonald, 1992; Davis & Shi, 1999; Sah et al., 2003). It is known to receive direct sensory input from the accessory olfactory bulb (Keshavarzi et al., 2014). Input from other amygdaloid nuclei originates mainly in the CeL (Davis et al., 2010) and the mITC cluster (Mańko et al., 2011). Its output projects mainly to hypothalamic regions (Keshavarzi et al., 2014). It is strongly associated with neuromodulatory and hormonal reactivity (Davis et al., 2010). Functionally it seems to be rather important for anxiety behavior (Davis et al., 2010) and innate emotional behavior (Keshavarzi et al., 2014).

Astr and IPAC. The Astr and the IPAC are anatomically not part of the amygdala as such, but closely linked to striatal or extended amygdala structures (Shammah-Lagnado et al., 1999). Concerning fear processing and even their anatomo-morphological properties, these regions are poorly investigated. The Astr is located medial to the IMC, between the CEA and the caudate putamen (CP). Depending on the rostro-caudal level, its lateral neighbor is the IPAC, the Globus pallidus (GP), the Stria terminalis or directly the IC (Franklin & George Paxinos, 2008). Cells located in the Astr are reported to be rather part of the striatopallidal complex (Shammah-Lagnado et al., 1999) and connected to basal ganglia as the Substantia nigra or the Globus pallidus (Shammah-Lagnado et al., 1996). The GP itself is connected to various brain regions including other nuclei of the basal ganglia, thalamic nuclei and brainstem areas (Shammah-Lagnado et al., 1996). One outgoing fiber tract of the GP is the Ansa lenticularis (AL) (Franklin & George Paxinos, 2008). The IPAC is positioned medial to the Astr and intimately related to the extended amygdala (Shammah-Lagnado et al., 1999), at least its medial part, which shows similar projection targets as the CeM (Shammah-Lagnado et al., 2001). Retrograde tracing reveals input from various amygdaloid regions including ITC clusters. Functionally, this region is thought to be implicated in regulating arterial blood pressure (Krémarik et al., 1995), as well as being closely related to other brain regions of autonomic

regulation (Shammah-Lagnado et al., 1999). In this thesis, these two regions will not be distinguished. If referred to the Astr region, both areas can be involved.

ITCs. The ITCs are GABAergic cells surrounding the BLA, grouped along the fiber bundles of IMC and EC in several distinguishable clusters (Millhouse, 1986; Marowsky et al., 2005)(1A and B). These cells and their known connectivity will be discussed in more detail.

1.3 Anatomy of intercalated cells (ITC)

In ontogenesis, ITCs become present at around embryonic day 13 (Cocas et al., 2009). They are thought to originate from the dorsal subdivision of the lateral ganglionic eminence as do medium spiny neurons of the striatum (Waclaw et al., 2010). This leads to the hypothesis, that ITCs are a ventro-medial extension of the striatum (Busti, 2012). ITCs are preserved over evolution and found throughout rodents, guinea pigs, cats, and humans. In mice, the ITC cells were recently revealed to be separable into six distinct clusters: (1) The mITC cluster situated ventro-medial to the BLA, (2) the lateral paracapsular (lpITC), located lateral of the BLA, (3) one cluster located inside the BLA in caudal parts of the amygdala, (4) another located supralateral on top of the LA, and (5 and 6) two clusters along the rostro-caudal axis of the IMC between the BLA and CEA, in this text referred to as one cluster, the mpITCs (Busti et al., 2011). These clusters contain ITCs with different morphological characteristics. The majority has small to medium size somata, whereas a minority shows large somata (L-ITC). The L-ITCs are located in the periphery of ITC clusters. They have a soma diameter of 40-60 μm and mostly aspiny dendrites (Millhouse, 1986; Busti et al., 2011; Bienvenu et al., 2015). Some of the L-ITCs express metabotropic glutamate receptor 1α (mGluR 1α) and receive inhibitory synapses from small ITCs (Busti et al., 2011). Recent results indicate that they also receive direct sensory input, so that they can relay noxious stimuli by making inhibitory synapses onto BLA cells (Bienvenu et al., 2012). The major group of ITCs possesses a somatic diameter of 9-18 μm and a mainly bipolar spiny dendrite tree (Millhouse, 1986). They are GABAergic and densely express μ-opioid (Jacobsen et al., 2006; Busti et al., 2011) and dopamin 1 receptors (Scibilia et al., 1992; Jacobsen et al., 2006). Therefore, ITCs are likely to be under neuromodulatory control. Concerning axonal distribution of the different ITC clusters, sparse knowledge is available. In general ITC axons were reported locally in the fiber bundles they are located in, as well as in the neighboring amygdaloid nuclei BLA, CEA and MEA (Millhouse, 1986; Mańko et al., 2011). Additionally, at least the mpITC and mITC cluster are interconnected (Busti et al., 2011; Mańko et al., 2011). In this thesis, if not otherwise stated, the focus will be on the group of small to medium size ITCs.

1.4 Connectivity of medial paracapsular ITCs (mpITC) and participation in different fear states

1.4.1 Connectivity of mpITC

Input. This cluster receives a major input from the BLA, providing glutamatergic synapses that can be altered by activity (Royer et al., 1999; Huang et al., 2014) and neuromodulators such as Neuropeptide S (Jüngling et al., 2008). Recent studies revealed that mpITCs also receive direct thalamic and cortical sensory input (Asede et al., 2015). It also is suggested that input is received from the mPFC, mainly the IL (McDonald et al., 1996; Berretta, 2005; Pinto & Sesack, 2008; Cho et al., 2013). However, this trajectory is still discussed due to recent contradictory results (Pinard et al., 2012; Dobi et al., 2013; Strobel et al., 2015).

Interconnectivity. Additionally, mpITCs are interconnected via GABAergic synapses in an inhibitory network with mainly unidirectional connectivity. Three different responding types in mpITC cell pairs have been shown depending on the presynaptic neuron that induces increasing, decreasing and constant synaptic transmission. These properties are thought to maintain stability of the network firing pattern (Geracitano et al., 2007).

Output. MpITCs project to the CEA (Pape & Pare, 2010) and could inhibit or disinhibit different CEA sub nuclei and subpopulations of cells depending on the entity of their postsynaptic partner (Duvarci & Pare, 2014). Studies in young animals show that their axonal projection pattern can also be diverse with different cell types projecting to CEA, the Astr, reaching in some cases the AL, and, to the mITCs. They make inhibitory synapses on neurons in these areas and onto large cells in the periphery of the ITCs, thought to be L-ITCs (Busti et al., 2011). Overall, mpITCs seem to be placed in a quiet strategic position - between the two amygdaloid main nuclei and along the amygdala entering fiber tracts - to receive and project to intra- and extraamygdaloid targets.

1.4.2 Participation of mpITCs in different fear states

MpITCs seem to be active during states of high and low fear. This was revealed by several immediate early gene mapping studies, as increased levels of the plasticity marker zif268 are seen after fear conditioning as well as after extinction learning. Further on, high levels of the activity marker c-fos were shown after extinction retrieval. And both, an increase of zif268 and c-fos were measured after impaired extinction retrieval (Hefner et al., 2008; Knapska & Maren, 2009; Whittle et al., 2010; Busti et al., 2011).

Low Fear. Participation in states of low fear is possible by exerting their long proposed role as inhibitory gate between the BLA and the CeM, thus reducing the fear response when they become active (Royer et al., 1999; Amano et al., 2010). Their activation is thought to occur via projections from extinction activated IL. MpITCs than inhibit CEA output (Cho et al., 2013; Duvarci & Pare, 2014). Behavioral evidence for their crucial role in extinction was provided by their pharmacological lesioning resulting in impaired extinction retrieval (Likhtik et al., 2008).

High Fear. Based on mpITC connectivity, participation in states of high fear has been suggested by two mechanisms. (1) Disinhibiting CeM output via inhibition of CeL neurons could trigger a behavioral fear response (Busti et al., 2011; Duvarci & Pare, 2014). (2) Another possibility is that activated ITCs could disinhibit CeM via inhibition of mITCs (Busti et al., 2011). Recent studies indicate that mpITCs themselves receive fear learning modulated sensory inputs (Asede et al., 2015).

In summary, mpITC activity seems to be associated with and important during states of high and low fear. However, the field is still lacking a connectivity model than can integrate all findings.

1.5 Aims of the thesis

This thesis aims at further revealing the neuroanatomical basis of mpITC connectivity to provide a better understanding of fear and extinction circuits. Using fluorescent and confocal imaging and immunohistochemical labeling as well as Neurolucida 3D cell reconstruction we address the following questions:

(1) Guided by the fact that efferent projections of mpITCs in young mice show an unexpected diversity (Busti et al., 2011), we want to assess which intra- and extraamgygdaloid regions are targeted by adult mpITCs.

(2) We aim to reveal if there is a distinct projection pattern of different mpITC projection types based on the axonal length in distinct target regions and if there are additional, more functional communication infrastructure parameters than axonal length.

(3) As mpITCs are known to project and make inhibitory synapses on cells in the IMC, Astr and CEA (Busti et al., 2011), we want to assess which cell population in the target regions receives putative mpITC synapses, focusing on the two functional opposing neuron populations in the CeL.

2 Materials and Methods

2.1 Chemicals and reagents

All chemicals, unless specifically stated otherwise, were reagent grade and obtained from Sigma-Aldrich (Hannover, Germany), Roth (Karlsruhe, Germany), Merck (Darmstadt, Germany), or VWR Prolabo (Darmstadt, Germany).

2.2 Animals and recordings for cell fills

Procedures with animals were all performed according with the EU directive for use of animals in experimental research and approved by the Regierungspräsidium Tübingen. Animals used in this study were male C57Bl/6-GAD67-Green Fluorescent Protein (GFP) knock-in mice aged six to ten weeks to identify GABAergic clusters and target ITCs for recording. In brief, acute life brain slices were obtained from these mice using standard procedures at a thickness of 320 μm. MpITCs were recorded via whole-cell patch-clamp recordings using an internal solution with 0.5% w/v biocytin, which allowed filling of the cells Asede et al. (2015). Recordings were performed by Dr. Douglas Asede in the Ehrlich laboratory.

2.3 Fixation and resectioning of amygdala acute slices

Upon completion of recording, slices with a biocytin filled cell were sandwiched between two filters to keep them flat and transferred to a fixative solution containing 0.05% glutaratalde-hyde in 4% paraformaldehyde in 1x phosphate buffered saline (PBS) and saturated picric acid solution for fixation at 4^{o}C overnight. Slices were washed three times in 1x PBS and stored at 4^{o}C until further use. For resectioning, the slices were embedded in 20% gelantine in deionized water and kept in fixative solution. Slices were recut with a HM 650v Vibrating Blade Microtome (Thermo Scientific, Karlsruhe, Germany) to 65 μm. The three to seven consecutive sections of one slice were kept in consecutive wells in a multiple well plate in 1x PBS at 4^{o}C until labeling within the following days.

2.4 Labeling slices of biotin filled mpITCs in fixed amygdala sections

The 65 μm slices were permebealized with 0.3% Triton in 1x PBS and the slices were incubated overnight at 4^{o}C with Cyan 3 (Cy3) or Cyan 5 (Cy5) fluorescently conjugated Strept

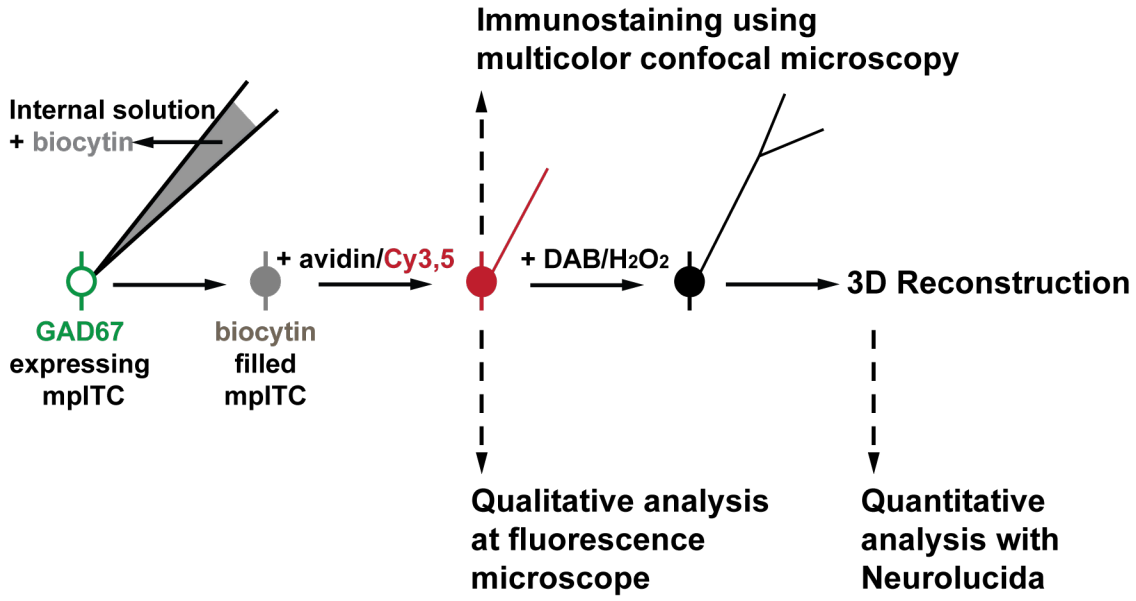

Figure 2: **Workflow of anatomical techniques**
Processing of amygdala slices coronal amygdala slices of adult (6-10 weeks) male C57Bl/6-GAD67-GFP mice containing filled mpITCs.

avidin (Life Technologies GmbH, Darmstadt, Germany) diluted at 1:1000 in 0.3% Triton in 1x PBS. The following day, the slices were washed three times in 1x PBS, mounted on 1-2 slides using Vectashield (Vector Laboratories, USA) as mounting medium and cover-slipped. The visualization of labeled cells with the fluorescent markers Cy3 and Cy5 was done at an Axio Imager 2 fluorescence microscope (Carl Zeiss, Jena, Germany). The microscope was connected to an AxioCAMMR3 camera (Carl Zeiss, Jena, Germany). Objectives used were Plan-Neofluar 5x/0.16NA, Plan-Neofluar 10x/0.30NA, Plan-Neofluar 20x/0.50NA and, Plan-Neofluar 40x/0.75NA. Two channel fluorescent images were taken and overlaid with the AxioCaMMR3 camera and AxioVision LE63 software (Carl Zeiss, Jena, Germany). I used the following filter sets: Cy3: BP 550/25, FT 570, BP 605/70; Cy5: BP640/30, FT660, BP690/50; GFP: BP 470/40, FT495, and BP 525/50.

2.5 Qualitative analysis of fluorescent labeled mpITC axonal projections

Cells were assessed for their axonal projection patterns after fluorescent revelation described above. Axonal projections of each cell were investigated in diverse intra- and extra amygdaloid target regions using multicolor fluorescent microscopy (Fig. 4A-E). Analyses were

performed in amygdala slices spanning from bregma position -1.22 to -1.94 according to the mouse brain atlas (Franklin & George Paxinos, 2008) (Fig. 3). Two to seven slices of 92 filled cells were imaged with 10x and 20x objective as described above, focusing on the axonal distribution. The following criteria were used to exclude samples: (1) the marker GFP was already bleached, (2) more than one cell body was labeled, (3) the labeled cell body was outside of the mpITC cluster, or (4) the filling or staining of the cell was not preserved in an sufficient manner (filled axonal length estimated <800 μm). After this preselection, 39 cells were confirmed as sufficiently labeled mpITCs in GFP-positive mpITC clusters. Excluded cells were not used for further analysis, except for samples with two somata in the mpITC cluster which were used for immunohistochemical staining. The axonal distribution of 39 cells was documented and the amount of axon estimated in each brain region, compared to the average diameter of the mpITC cluster of ca. 100 μm. The axonal amount in each target region was encoded qualitatively with numbers (0-3) indicating no, low, middle and high amount of axon, respectively. Numbers from 0-3 were additionally color coded (green to red). The bregma level of the slice containing the cell body was defined using the mouse brain atlas (Franklin & George Paxinos, 2008) (Fig.3). This procedure was done in the same manner for a larger amount of mpITCs in the Ehrlich laboratory (additional 80 cells).

2.6 Diaminobenzidine (DAB) peroxidase staining of mpITC samples

To obtain permanent, light stable samples for cell reconstruction, the fluorescently labeled cells were converted using Avidin-Biotin (ABC) Elite kit (Vector Laboratories, USA) and diaminobenzidine (DAB)peroxidase. The conversion steps were done on slide, and solution prevented from dropping off the slide by Neovanish lines on the slide borders. Sections were incubated for three hours at room temperature (RT) with 1:100 B-Component in 0.3% Triton in 1x PBS. After washing (3x) sections were incubated with 1:100 A-B-Component in 0.3% Triton in 1x PBS. The diluted A-B Component had to react for 30 minutes at RT before usage. The following day, slices were washed in 0.3% Triton in 1x PBS and incubated with DAB peroxidase in deionized water for 5-10 minutes. The reaction was monitored after reaction break at Leica light microscope (Leica, Wetzlar, Germany) to confirm a sufficient axonal and dendritic visualization. The slices were dried in air for 15 minutes and maintained for five minutes in ascending alcohol series (50%, 70%, 75%, 90% 95%), and, for ten minutes in 100% alcohol and xylol. The slide was immediately cover-slipped with Entellan embedding medium and dried under the hood overnight.

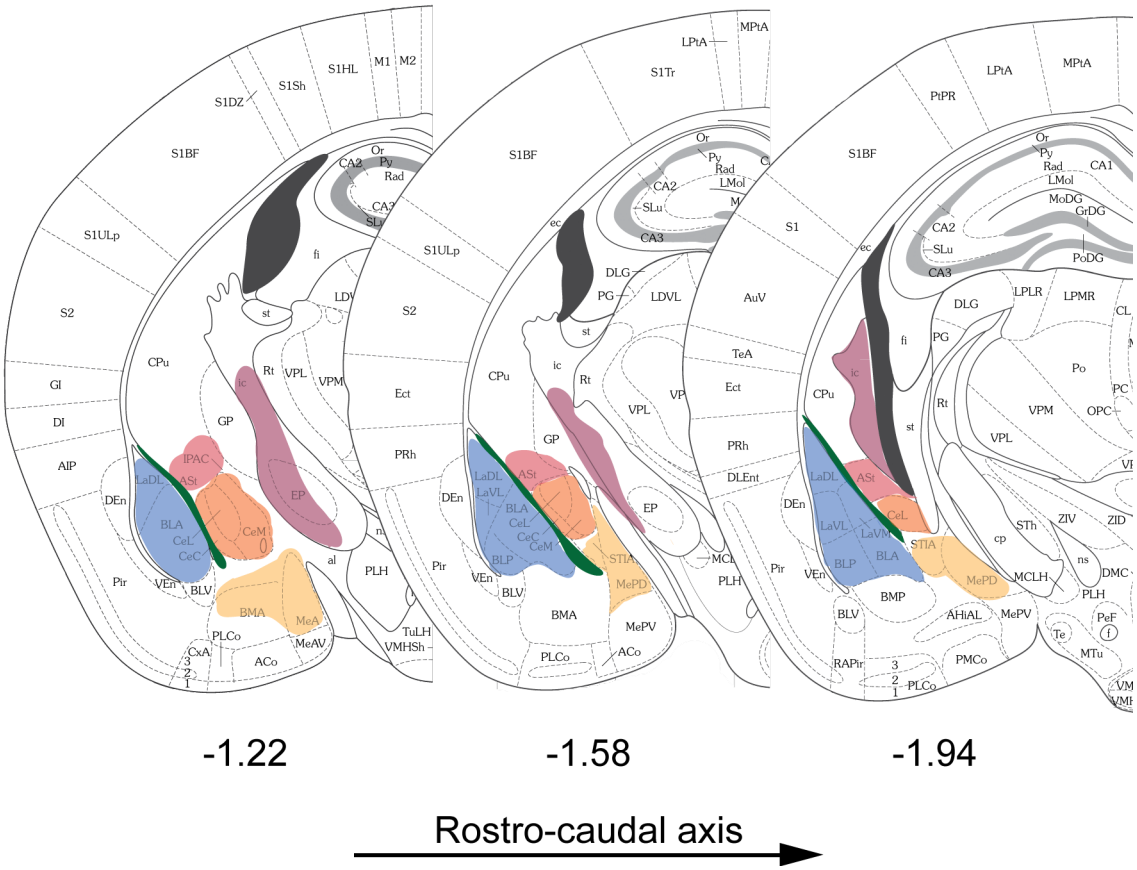

Figure 3: **The amygdaloid nuclei along the rostro-caudal axis**
Shown is the shape of brain nuclei in coronal slices at the amygdala containing bregma levels -1.22, -1.58 and, -1.94. Highlighted are amygdaloid and adjacent nuclei as the BLA (in blue), the CEA (in orange), the Astr (in pink), the MEA (in yellow) and fiber tracts as the IMC (in green) and the IC (in magenta). This color code is used throughout the thesis. Images were adapted from the mouse brain atlas (Franklin & George Paxinos, 2008).

2.7 3D-reconstruction of DAB samples with Neurolucida software

3D-reconstruction was performed in a subset of the qualitatively analyzed cells subsequent to DAB conversion. Criteria for reconstruction were 1) preservation of all consecutive sections of the cell and 2) cells spanning at least over 3 sections. Reconstruction was performed at the Neurolucida-System (version 10 from MBF Bioscience, USA) coupled to an Olympus BX 53 Light Microscope and Olympus U-CMAD 3 Camera (Olympus Corporate, USA). Coronal brain slice contours and different brain structures were traced under Plan Neofluar 2x, NA 0.06 and Plan Neofluar 10x, NA O.25 objectives based on contrast and cell morphology in the different regions. ITC clusters were detectable as they appear as dense cluster with small cell bodies in the fiber tracts around the BLA. The magnocellular BA was distinguishable from LA by cell body size and in part by fibers from the EC passing along this border. The CEA appears as a round structure containing smaller cell bodies than the BLA. Different subdivisions were selected if possible by contrast difference and in part by fibers passing from medially at the CeL/CeM border. The Astr-CP dividing contour was reconstructed halfway between the tip of LA and the most dorsal point of the CEA in a 90ř angle to the IMC-axis. This was necessary as a clear anatomical border is mostly not detectable between the two structures and it is in good agreement with the Allen mouse brain atlas. If the shape of the CP was detectable, the tip of it was used to draw a tangent at a 90ř angle to IMC axis. Z-level of all contours was set equally in each section. Cell structures including cell body, dendrites, axons and axonal parameters such as branchpoints and varicosities were traced in 3D with an Olympus N340 40x, NA 1.15 water objective for each section in each cell sample. For a full 3D-reconstruction of all subsequent sections as seen in Figure 15 and 16, axons and dendrites were spliced in the Ehrlich laboratory in each section if the gap between ending and starting point was not more than 15 μm in the x and y-axis and 35 μm in the z-axis apart. For intersection splicing, the z-axis gap was not more than 30 μm.

2.8 Analysis of reconstructed samples with Neurolucida Explorer

Different axonal parameters, such as axonal length, branchpoints, and varicosities of reconstructed sections were quantitatively analyzed for each target region, subsequent to 3D-tracing (without splicing), with the Neurolucida Explorer (version 10 of MBF Bioscience). Analyses performed were the “Branched Structure Analysis” including the “Neuron Summary” and the “Marker on Segment-Axon” tool to obtain the amount of axon, the axonal length, and the amount of varicosities. To depict the branching pattern and the axons ac-

tual branchpoints, a dendrogram of the region containing axons was obtained. Results were exported to Microsoft Excel or Power Point, respectively, and finally subjected to further statistical analysis.

2.9 Immunohistochemical staining of neuron populations in mpITC target regions

To assess putative mpITC postsynaptic targets, fluorescently labeled slices containing mpITC axon were stained with a number of immunohistochemical markers. A list of all primary antibodies and dilutions is provided in Table 1. Subpopulations of L-ITCs in the periphery of ITC clusters express mGluR1α (Busti et al., 2011; Bienvenu et al., 2015) and another subpopulation may express Neurokinin-1 (NK-1) Receptor (Busti, 2012). Thus, we used mGluR1α and rabbit NK-1 Receptor as marker to identify these cells. To identify the two major cell populations in the CeL, we stained slices for PKC δ and/or SOM. Cholinergic interneurons in the striatum show positive immunoreactivity for choline acetyl transferase (ChAT). To reveal this cell population, we stained for ChAT. If possible, co-staining was attempted with Gephyrin, a postsynaptic marker for inhibitory synapses. Sections with axon in specific target regions were selected and labeled for one or two of the immunohistochemical markers in this region. Selected slices were unmounted, permebealized with 0.3% Triton in 1x PBS and blocked with 20% normal goat or normal horse serum, depending on the secondary antibody used, for 90 minutes at RT. Then, slices were incubated with primary antibody in 2% blocking serum for 72 hours at 4^{o}C. Afterwards, slices were washed with 0.3% Triton in 1x PBS and incubated with the appropriate anti-species secondary antibodies conjugated with infrared (633 nm/ 647 nm) Alexa dye and/ or ultraviolet (405 nm) Alexa dye in 2% blocking serum overnight. Dilution for all secondary antibodies was 1:1000. The same protocol was applied as control staining without primary antibody. After washing with 0.3% Triton in 1x PBS slices were mounted, cover-slipped with Vectashield or ProLong Diamond Antifade (Life Technologies, Darmstadt, Germany) mounting media and the coverslip was closed by nail polish.

Table 1: **List of primary antibodies used**

Antibody	Antigen	Species	Dilution	Source
ChAT	human placental enzyme	goat	200	Chemicon, catalog# AB144P
Gephyrin	recombinant doublet of E-Domain/C6 Domain located in the first half of the E-Domain	mouse	150	Synaptic Systems, catalog# 147 021
mGluR1α	KLH-conjugated, synthetic peptide corresponding to amino acids 1180-1199 of rat mGluR1. The immunizing sequence is identical in mouse	rabbit	500	Millipore, catalog# 07-617
NK-1	synthetic peptide that corresponds to a 23 amino acid sequence (385-407) of the COOH-terminus of the rat substance P Receptor (NK-1)	rabbit	500	Chemicon, catalog# AB5060
PKC δ	human PKC δ aa, 114-289	mouse	1000	BD Bioscience catalog# 611461
SOM	synthetic peptide	rabbit	1000	Bachem, catalog# T-4547

2.10 Multicolor Confocal Laser Microscopy of mpITC putative postsynaptic contacts

Subsequently to immunohistochemical staining, slices were imaged using a Zeiss LSM 710 multicolor confocal laser scanning microscope (Carl Zeiss, Jena, Germany). All images were acquired using the 63x oil 1.4 NA objective in single area or tile scan mode at 0.6-1.3x zoom. Pinhole size was set equally for all channels, and adjusted to one airy unit. Laser wavelengths used, were 405 nm for ultraviolet dyes (Alexa 405), 488 nm for GFP, 561 nm for red dyes (Cy3), and, 633 nm for infrared dyes (Alexa 633, Alexa 647 and Cy5). Images containing appositions of mpITC axon on putative postsynaptic partner structures were imaged as z-stack with an optical thickness of 0.49-0.51 μm and analyzed at ZEN software (2012, black and blue edition, Carl Zeiss, Jena, Germany).

2.11 Statistics

For numeric data, all data are presented as mean ś standard error of the mean (SEM). Nominal data were compared with Pearson's Chi^2 Test, as in Figure 6 A2 or Exact Fisher's Test as in Figure 8 B2. Group comparisons of numeric data were performed using one-way ANOVA (OWA) as in Figure 9 A2, followed by Tukey-HSD Post Hoc Test as in Figure 12. To analyze the relationship between two numeric variables, regression analysis was used in a linear model, as fitting in Figure 10 and 11. The trendline was not layed through 0. To identify the significance of the regression model, an F-Test was performed. Correlation levels are indicated by adjusted coefficent of determination (r^2) values. Correlation coefficients (r) were tested to be significantly different from 0. For all tests, data were considered to be significantly different when $p < 0.05$. All statistical analyses were performed using the software SPSS (IBM, USA).

3 Results

3.1 Qualitative assessment of projection patterns of adult mpITCs based on fluorescence microscopy

To obtain a qualitative assessment of fluorescently labeled mpITC projections in coronal amygdala slices, single mpITCs were analyzed for their axonal distribution patterns subsequent to reslicing, fluorescent staining, and preselection. Only sufficiently labeled mpITCs in GFP-positive mpITC clusters were used as described in more detail under methods (2.5). As my thesis is part of a larger project in the lab about mpITC output, in part 3.1 the results of the dataset analyzed by myself are shown (n = 39 mpITCs) including cells for which I performed the entire preparation and analysis. To obtain a more complete picture, I also show results of the entire dataset available in the lab (n = 119 mpITCs) containing additional cells for some of which I participated in the projection analysis.

3.1.1 Qualitative analysis of efferent projection patterns in individual cells

The initial examination of single filled mpITCs was performed at the fluorescent microscope to assess where mpITCs project to and which proportion of single cells sends axon collaterals to different designated target regions. In this initial examination, it immediately became apparent, that individual ITCs have quite diverse projection patterns. This is illustrated in Figure 4, in which example images of labeled cells in GAD67-GFP mice in coronal amygdala slices are shown. Firstly, an exemple of a cell is shown that sends axon collaterals to the IMC as well as to the BLA, and another major branch traveling through the CEA to reach the Astr (Fig. 4 A). Secondly, cells are observed that show axon collaterals in the mpITC cluster and a major projection through the Astr reaching fiber bundles of the IC (Fig. 4 B). Thirdly, an exemple of a cell is depicted with axon in the IMC, a shorter piece in the BLA, and a long axon collateral that extends through the CEA and further medioventrally in direction to the MEA (Fig. 4 C). Fourthly, an mpITC is shown with axon in the mpITC cluster and a more extensive arborization in the CEA (Fig. 4 D). Lastly, an mpITC is shown with axon mainly in the IMC, traveling ventral to arbor vastly in the mITC, as well as small axon collaterals in the BLA and CEA (Fig. 4 E). To get a more complete picture of this apparent diversity, I analyzed the target areas and projection complexity. In a first approach, I asked which percentage of cells projects to a given target region, independently of the length of axons in this area (Fig. 5 A1). This revealed that all analyzed mpITCs ramify locally in the IMC.

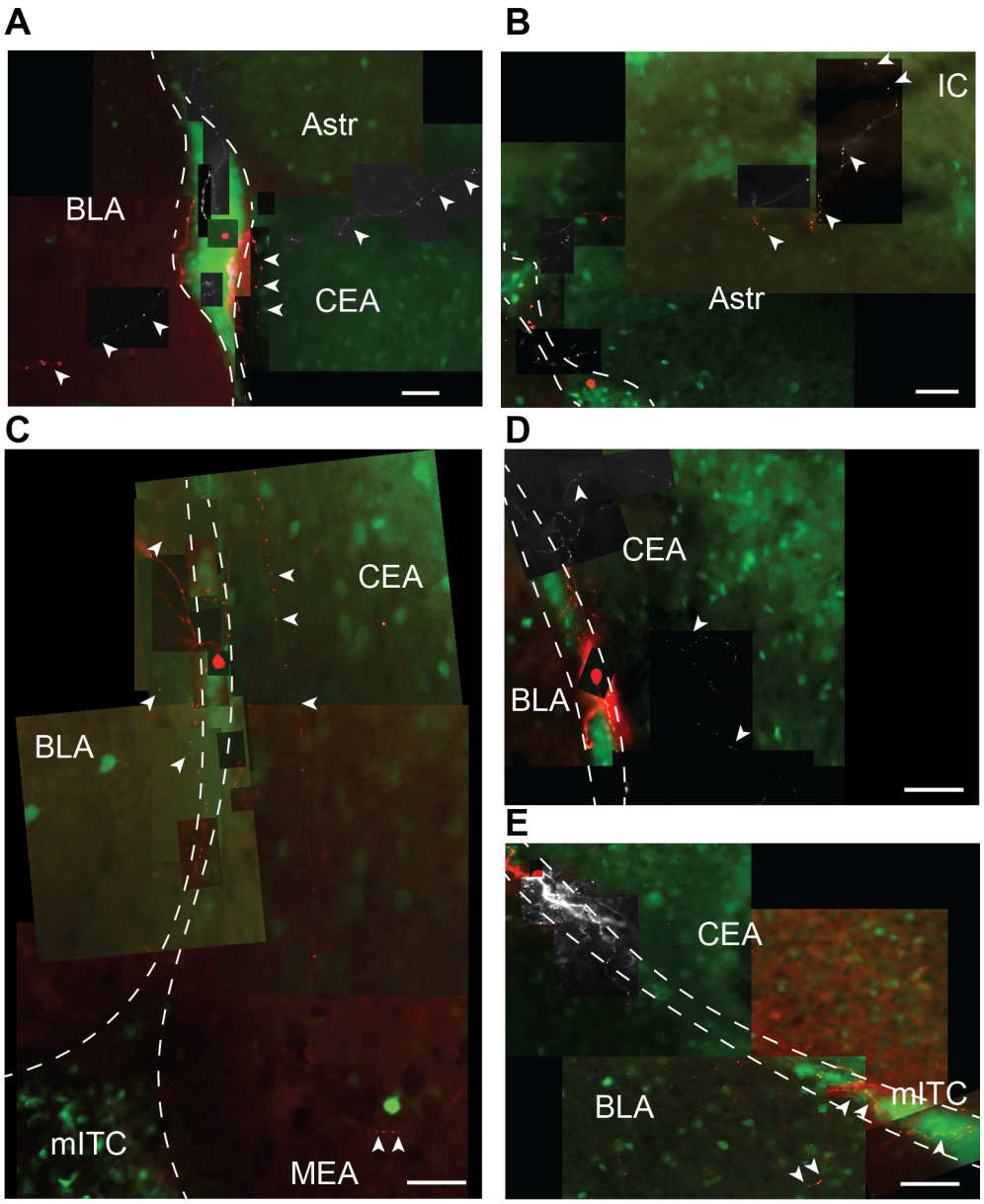

Figure 4: **Images of fluorescently labeled mpITCs projecting to amygdaloid and adjacent nuclei** (A-E) Fluorescent images of coronal amygdala slices of GAD67-GFP young adult mice containing Cy3- or Cy5-labeled single mpITCs. GABAergic neurons containing GFP. The images are created from several images that differ in focus depth, are from consecutive tissue sections, and were imaged with one or two channels (two channel images: GFP in green, Cy3 or Cy5 in red; one channel images: Cy3 or Cy5 in white). Scale bars for all panels: 50 μm. White arrowheads point to pieces of axon in specific target regions. Dotted line denotes the borders of the IMC. (A) Example of an mpITC with axonal ramifications in the IMC, the BLA, the CEA and some in the Astria. (B) Example of an mpITC with axonal ramifications in the IMC, the Astr and the IC. (C) Example of an mpITC with axonal ramifications in the IMC, the BLA, some in CEA and a long axon traveling to the MEA. (D) Example of an mpITC with axon in the IMC and more extensive axonal arbor in the CEA. (E) Example of an mpITC with axonal ramifications in the IMC, ventral into the mITC, and BLA.

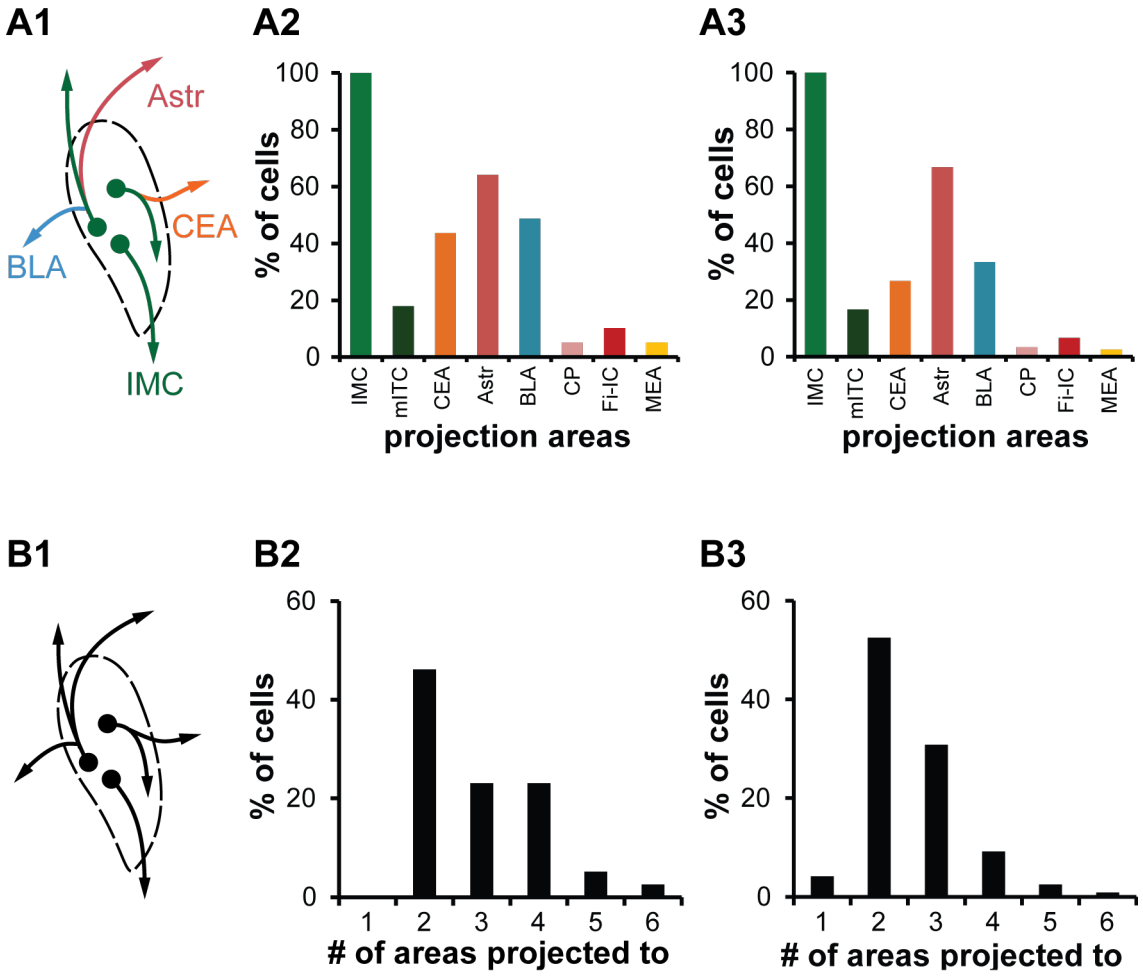

Figure 5: **Heterogeneity in target regions and complexity of projection patterns of mpITCs of young adult mice**

(A1-3) Analysis of the frequency with which different areas are targeted by mpITCs. (A1) Scheme of individual mpITCs with different projection patterns and the principle of the analysis. (A2-3) Shown is the percentage of mpITCs that target specific projection areas. (A2) Dataset with n=39 cells. The relative numbers of cells sending axons to an individual target are IMC: 100%, mITC: 17.5% CEA: 43.6%, Astr: 64.1%, BLA 48.7%, CP: 5.1%, Fi-IC: 10.3%, and MEA: 5.1%. (A3) Complete dataset with n=119 cells (data from A2 included). The relative number of cells sending axons to an individual target region is for IMC: 100%, mITC: 16.8%, CEA: 28.6%, Astr: 67.2%, BLA: 33.6%, CP: 3.4%, Fi-IC: 5.9%, and MEA: 3.4%. (B1-3) Analysis of complexity, i.e. the number of areas reached by axon collaterals of individual mpITCs (B) Scheme of individual mpITCs with the number of major projections, illustrating the principle of the analysis. (B2-3) Complexity distribution of single mpITCs. (B1) Dataset with n=39 cells. Cells with projections to one target region: 0%, two target regions: 46.15%, three and four target regions: 23.08% each, five target regions: 5.13%, and six target regions: 2.56%. (B2) Dataset with n=119 cells (data from A1 included). Cells with projections to one target region: 4.2%, two target regions: 49.6%, three target regions: 32.8%, four target regions: 10.9%, five target regions: 1.7%, and six target regions: 0.8%.

The additional main target regions are in descending order the Astr, the BLA, and the CEA (Fig. 5 A2 and A3). The target regions that receive projections less frequently include the mITC, as well as additional regions such as the CP, the IC, and the MEA. This heterogeneous axonal distribution pattern looked very similar in the small (Fig. 5 A2) and the large dataset (Fig. 5 A3). Until recently, the BLA was not reported to receive projections of mpITCs in this extend. The functional role of these projections is further investigated in a parallel study from our lab (Asede et al., 2015). The previous data also suggests that single mpITCs can project to more than one target area. In a second analysis, I asked how many areas are targeted by single cells, as a first crude measurement of projection complexity (Fig. 5 B1). This revealed that about half of the analyzed mpITCs send axon collaterals to at least two different target regions, the IMC and an additional one. A substantial number (more than 25% of cells) sends axons to three or more areas, with a small number of cells targeting even up to six regions (Fig. 5 B2 and B3). The complexity distribution of the small (Fig. 5 B2) and large dataset (Fig. 5 B3) looked overall similar.

Taken together, this qualitative analysis suggested projection complexity for single mpITCs in young adult mice. The patterns were more heterogeneous including multiple and more diverse target regions than previously reported.

3.1.2 Qualitative analysis of efferent projection pattern of total cluster output

Next, my goal was to assess the total output of mpITC cluster along the rostro-caudal axis, to depict the clusters' projectional impact on target regions, as well as its similarity along the rostro-caudal axis. Towards this end, I analyzed the clusters' output as all projections found at each bregma level irrespective of their cell origin (Fig. 6 A1). Analysis was performed in the large dataset. Results showed in Figure 6 A2 that the total cluster output is not significantly different along the rostro-caudal axis with the main projectional impact of the whole cluster in the IMC and Astr (Pearson's Chi^2 Test, $p = 0.852$). Additionally, I looked at the rostro-caudal distribution of complexity (i.e. number of target areas) to check for similarities of this pattern at different bregma levels. Results showed a distribution of the number of target areas taht seems to stay similar along the rostro-caudal axis with mainly two or three target areas at all bregma levels (Fig. 6 A3).

Overall, these analyses indicated homogeneity of the total cluster output and complexity of projections of the mpITC cluster along the rostro-caudal axis. This suggested that the cluster

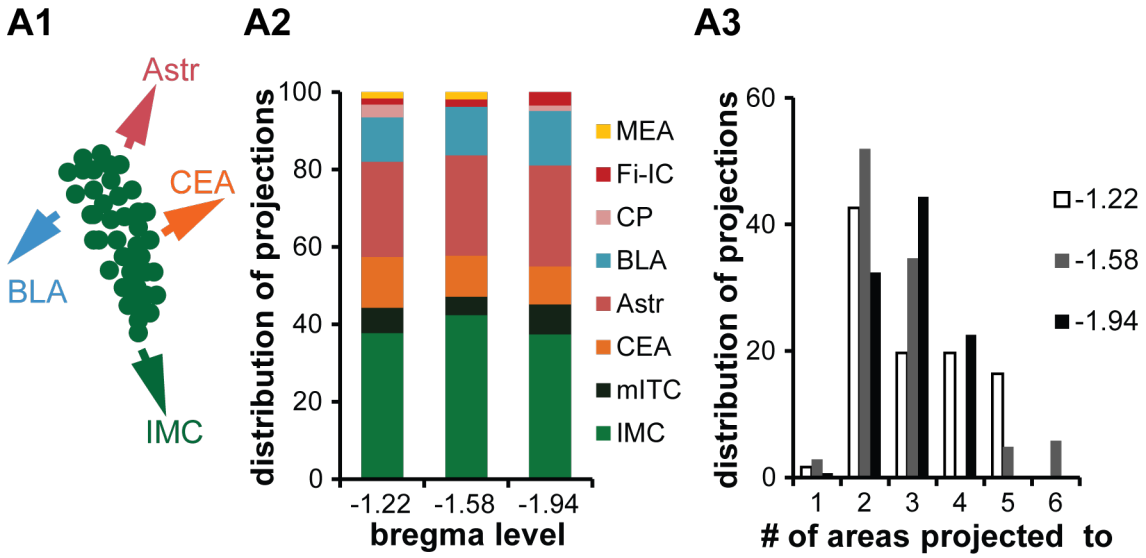

Figure 6: **Homogeneity of total cluster output along the rostro-caudal axis**
(A1) Scheme of total mpITC cluster output e.i. all projections of the whole cluster to designated target regions irrespective of their cell origin. (A2-3) Dataset with n=305 projections of 119 cells, at bregma level -1.22 mm: n=61 projections, -1.58 mm: n=104 projections, -1.94 mm: n=140 projections. (A2) Distribution of all projections of the mpITC cluster to designated target regions along the rostro-caudal axis. The relative numbers of projections to an individual target are at bregma level – 1.22mm: IMC: 37.7%, mITC: 6.6%, CEA:13.3%, Astr: 24.6, BLA: 11.5%, CP: 3.3%, Fi-IC: 1.6%, MEA: 1.6%; at bregma level -1.58mm: IMC: 42.3%, mITC: 4.8%, CEA: 10.6%, Astr: 26.0%, BLA: 12.5%, CP: 0.0%, Fi-IC: 1.9%, MEA: 1.9%; at bregma level -1.94mm: IMC: 37.1%, mITC: 7.9%, CEA: 10.0%, Astr: 25.7%, BLA: 14.3%, CP: 1.4%, Fi-IC: 3.6%, MEA: 0.0%. Pearson's $Qui^2(14)=8.664$, p=0.852. (A3) Distribution of projection complexity along the rostro-caudal axis. The relative numbers of projections were at bregma level -1.22 mm 1 area: 1.6%, 2 areas: 42.6%, 3 and 4 areas: 19.7% each, 5 areas: 16.4%, 6: 0.0%; at bregma level -1.58 mm 1 area: 2.9%, 2 areas: 51.9%, 3 areas: 34.6%, 4 areas: 0.0%, 5 areas: 4.8%, 6 areas: 5.8%; at bregma level -1.94 1 area: 0.7%, 2 areas: 31.4%, 3 areas: 45.0%, 4 areas: 22.9%, 5 areas: 0.0%, 6 areas: 0.0%.

as whole can exert a similar impact onto different target regions at different rostro-caudal positions.

3.1.3 Qualitative classification of putative projection types

As different cell types have been described in young animals (Busti et al., 2011), my next goal was to obtain first insights into putative projection types from my qualitative analysis in adult animals. The classification criteria were adapted from an unsupervised cluster analysis previously done in young animals (Busti et al., 2011). My criteria included the extent

A1

axon in targeted areas

projection types	IMC	mITC	CEA	Astr	BLA	CP	Fi-IC	MEA
IMC	1.57	0.48	0.52	0.52	0.43	0.00	0.00	0.04
CEA	1.50	0.00	1.50	1.00	0.00	0.00	0.00	0.00
Astr	1.75	0.00	0.25	2.13	0.50	0.25	0.38	0.00
BLA	1.25	0.00	0.00	0.50	1.75	0.00	0.00	0.00
Fi-IC	1.00	0.00	0.00	2.00	1.00	0.00	1.00	0.00
MEA	2.00	0.00	1.00	0.00	1.00	0.00	0.00	1.00

A2

axon in targeted areas

projection types	IMC	mITC	CEA	Astr	BLA	CP	Fi-IC	MEA
IMC	1.87	0.47	0.42	0.47	0.33	0.00	0.00	0.04
CEA	1.56	0.11	1.56	0.78	0.00	0.00	0.00	0.00
Astr	1.50	0.08	0.10	1.68	0.18	0.08	0.05	0.00
BLA	1.44	0.13	0.19	1.06	2.00	0.00	0.00	0.00
CP	1.00	0.00	0.00	1.00	0.00	1.00	0.00	0.00
Fi-IC	1.00	0.20	0.00	0.40	0.20	0.00	1.60	0.00
MEA	2.00	1.50	0.50	0.00	0.50	0.00	0.00	1.50

B1 **B2**

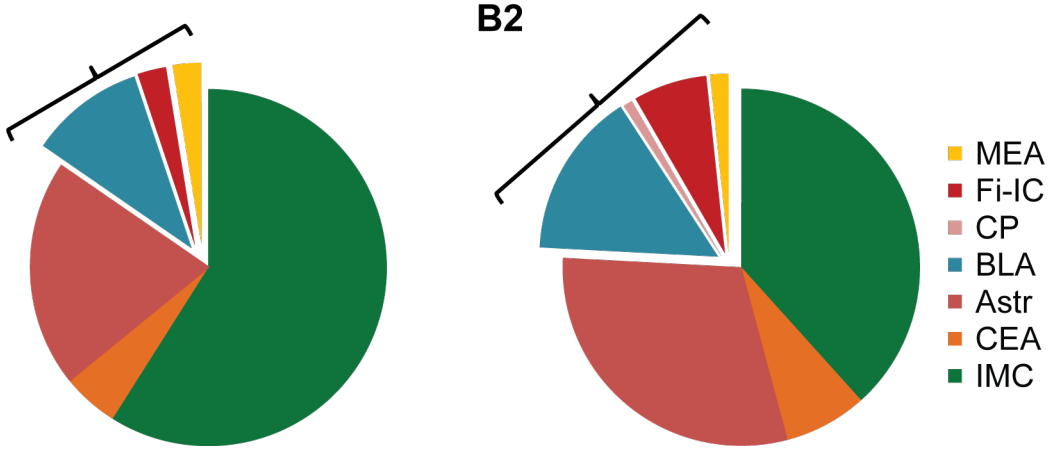

Figure 7: **Qualitative categorization of projection types in young adult animals**
(A1-2) Qualitative distribution of average axonal projections in different target areas sorted by putative projection cell type (scale from 0 to 3). More red colors indicate larger amounts of axon. (A1) Dataset of n=39 cells. (A2) Dataset of n=119 cells. (B1-2) Relative contribution of putative projection cell types to the overall population of cells. (B1) Dataset of n=39 cells. IMC projection type: 59.0%, CEA projection type: 5.1%, Astr projection type: 20.5%, BLA projection type: 10.3%, Fi-IC projection type: 2.6%, MEA projection type: 2.6%. (B2) Dataset of n=119 cells. IMC projection type: 37.8%, CEA projection type: 7.6%, Astr projection type: 33.6%, BLA projection type: 14.3%, CP projection type: 0.8%, Fi-IC projection type: 4.2%, MEA projection type: 1.7%.

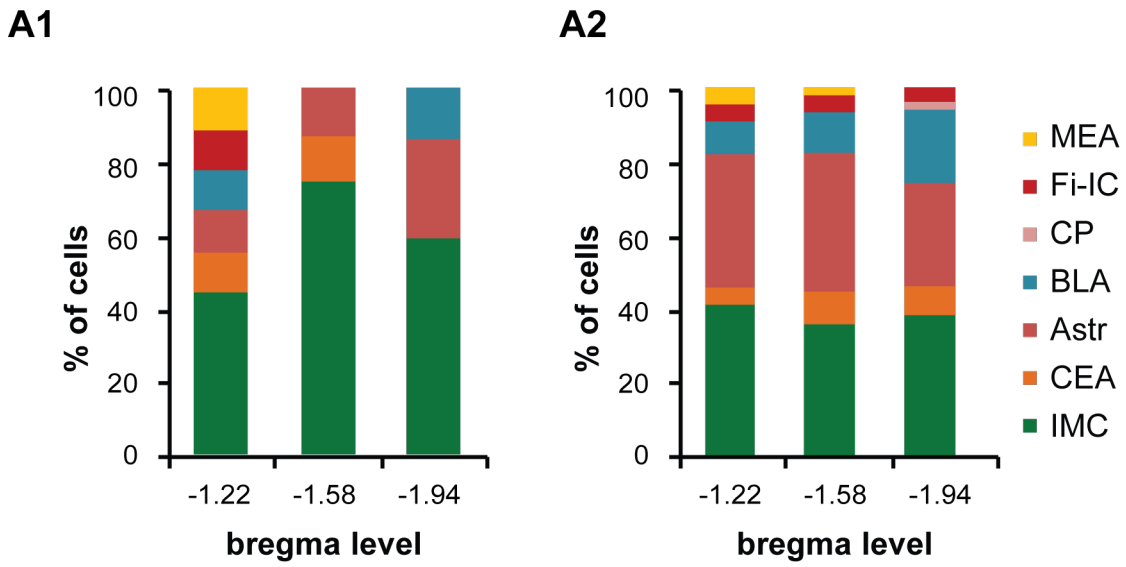

Figure 8: **Distribution of projection types along rostro-caudal axis**
(A1-2) Distribution of putative projection types along the rostro-caudal axis. (A1) Dataset of n=39 cells. Bregma -1.22 mm: n=9 cells; IMC projection type: 44.4%, CEA, Astr, BLA, Fi-IC and, MEA projection type: 11.1%. Bregma -1.58 mm: n=8 cells; IMC projection type: 75.0%, CEA and, Astr projection type: 12.5%, BLA, Fi-IC and MEA projection type: 0.0%. Bregma level -1.94 mm: n=22 cells; IMC projection type: 59.1%, CEA projection type: 0.0%, Astr projection type: 27.3%, BLA projection type: 13.3%, Fi-IC and MEA projection type: 0.0%. (A2) Dataset of n=119 cells. Bregma level -1.22 to -1.34 mm: n=23 cells; IMC projection type: 39.1%, CEA projection type: 4.3%, Astr projection type: 39.1%, BLA projection type: 8.7%, CP projection type: 0.0%, Fi-IC projection type: 4.3%, MEA projection type: 4.3%. Bregma -1.58 mm: n=45 cells; IMC projection type: 35.6%, CEA projection type: 8.9%, Astr projection type: 37.8%, BLA projection type: 11.1%, CP projection type: 0.0%, Fi-IC projection type: 4.4%, MEA projection type: 2.2%, Bregma -1.82 to -1.94 mm: n=51 cells; IMC projection type: 39.2%, CEA projection type: 7.8%, Astr projection type: 27.5%, BLA projection type: 19.6%, CP projection type: 2.0%, Fi-IC projection type: 3.9%, MEA projection type: 0.0%. Exact Fisher's Test=7.202, p=0.9.

(estimated axon length in distinct target region) and final destination of the axon. The projection strength is the estimated axonal length categorized into low, middle, and high, indicated by numbers (1, 2, and, 3) and visualized by green-red color code (Fig. 7 A and B). The average estimated amount of axon in each target region of each putative projection type is plotted in Figure 7 A. Again, the small dataset (Fig. 7 A1) looks similar to the large dataset (Fig. 7 A2). We identified around 3/4 of our cells as IMC-projecting (IMC-p), CEA-projecting (CEA-p), and Astr-projecting (Astr-p) types, targeting preferentially these regions, each additionally to the IMC. These projection types resemble cell types reported in young animals.

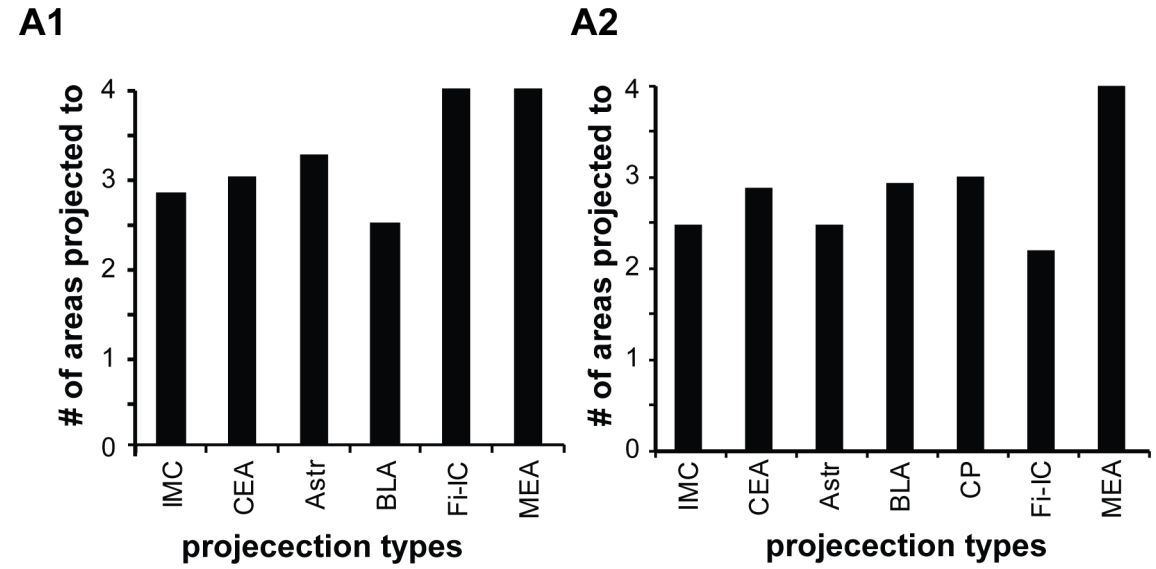

Figure 9: **Homogeneity of average complexity in all projection types**
(A1-2) The average complexity, as number of areas projected to, appears homogeneous among putative projection cell types. (A1) Dataset of n=39. Average numbers of projection areas and SEM were: IMC type: 2.8 $\pm$ 0.25 (n=23), CEA type: 2.9 $\pm$ 0.21 (n=9), Astr projection type: 2.5 $\pm$ 0.11 (n=40), BLA type: 2.5 $\pm$ 0.33 (n=4), Fi-IC type 4.0 (n=1), MEA type: 4.0 (n=1). (A2) Dataset of n=119. Average numbers of projection areas and SEM were: IMC type: 2.49 $\pm$ 0.16 (n=45), CEA type: 3.0 $\pm$ 0.00 (n=2), Astr projection type: 3.3 $\pm$ 0.39 (n=8), BLA type: 2.9 $\pm$ 0.15 (n=16), CP type: 3.0 (n=1), Fi-IC type 2.2 $\pm$ 0.22 (n=5), MEA type: 4.0 $\pm$ 1.41 (n=2). OWA: F(6;112)=1.886, p=0.089.

Around 1/5-1/4 of analyzed cells did not resemble cell types reported before, suggesting possible new projection types to the BLA, the MEA and the IC (Fig. 7 B1 and B2). Next, I assessed if the distribution of different projection types was homogeneous along the rostro-caudal axis. And it was statistically not different along all analyzed bregma levels in the large dataset (Exact Fisher's Test; p = 0.9, Fig. 8 A2), whereas in the small dataset, not all projection types were present at all rostro-caudal levels, what was probably due to low n numbers (Fig. 8 A1). Further on, to get a first impression of the complexity of different projection types, the average number of target areas was calculated from all putative projection types. My results showed, that on average each projection type targets more than two areas (Fig. 9 A1 and A2) and this number was statistically similar for all projection types (OWA, p = 0.089, Fig. 9 A2). The slight trend in the small dataset towards a higher complexity of projection types with more distant final target regions (Fig. 9 A1) was only partly seen in the large dataset (Fig. 9 A2).

Taken together, the major finding from this analysis was, that putative projection types re-

sembling cell types reported in young animals (Busti et al., 2011) are present in young adult animals, too. Additionally, putative new projection types to the BLA (Asede et al., 2015), and possibly the MEA and the IC may exist. Moreover, all projection types were detectable similarly along the rostro-caudal axis and exhibited a similar complexity in the number of regions that are targeted.

3.2 Quantification of axonal parameters in distinct target regions using Neurolucida 3D-reconstructed mpITCs

In a subset of qualitatively analyzed mpITCs (n = 10), I performed a time consuming 3D-reconstruction and quantification of axonal parameters such as axonal length, branchpoints and varicosities. Two of these cells were reconstructed during a visit in the lab of a collaborator Prof. Dr. Ferraguti, (Medical University of Innsbruck). Michaela Richter, an intern in the Ehrlich laboratory also participated in the reconstruction under my supervision of two of these cells.

3.2.1 Analysis of axonal parameters to define axonal communication infrastructure

To gain more precise and functional insights into the impact of mpITCs axons in different target regions, we wanted to quantify axonal communication infrastructure in addition to axonal length. The first infrastructural parameter analyzed was the density of branchpoints. A typical branchpoint diagram as visible in Neurolucida Explorer is shown in Figure 10 A. The idea behind analyzing this parameter was that higher density of branchpoints could indicate that more local communication is possible, whereas a lower the density of branchpoints could indicate a passing axon through this area and that more communication maybe takes place in an area further away. First, I wanted to see if density of branchpoints as measured here, is a reliable parameter usable to compare the density of axon pieces of different length. A linear regression model was used to test if there exists a linear relationship between branchpoints and length, even for very short and long axon pieces. I found a significant correlation between axonal length and amount of branchpoints using data from all the different target regions (adjusted $r^2 > 0.7$, $p < 0.001$; Fig. 10 B). Nevertheless, almost half of all axon pieces did not show branchpoints at all (Fig. 10 B2). These axon pieces measured < 300 μm and were dispersed over all target regions, distant and close ones (data not shown). However, making a cut off for short axons does not seem plausible as around 50% of axon pieces with < 300 μm showed branching (Fig. 10 B2). Thus, it was difficult to distinguish if no branchpoint indicated axon pieces too short to branch or passing axons in the area. Therefore, this parameter did not seem to be a good choice to describe the axon's functional impact in a distinct target region and was not analyzed further. The second parameter analyzed was the density of varicosities. Varicosities most likely present the presynaptic units along the axon that release neurotransmitter in the target areas (Trepel Martin, 2008; Bear F. Mark et al., 2008). A typical branchpoint diagram with several varicosities as visible in Neurolucida

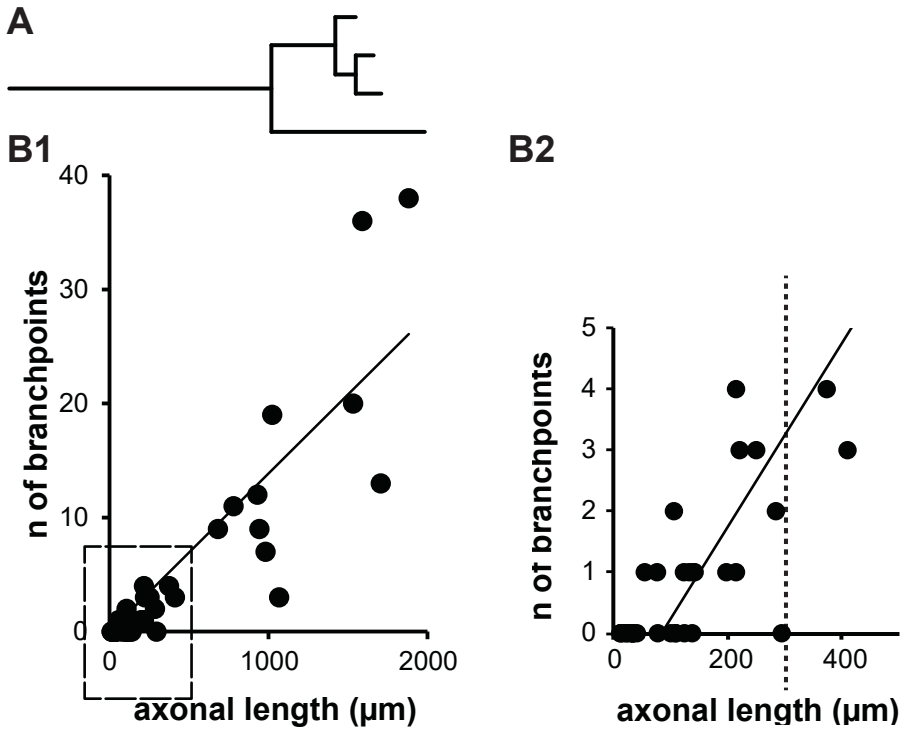

Figure 10: **Axon parameters: branchpoints analysis over all regions**
(A) Scheme of a branching axon (dendrogram) showing three branchpoints. (B1-B2) Dataset of n=44 regions targeted by 10 cells. The graphs show the number of branchpoints as a function of axonal length in all target regions. Linear regression analysis shows a highly significant correlation between branchpoints and axonal length, $F(1,42)=156.986$, $p<0.001$, adj. $r^2= 0.784$. (B2) Graph is a zoom in of graph B1, indicated by dotted frame, showing 33/44 branchpoints. Dotted line indicates $300\mu m$ on the x-axis, 18/44 of axon pieces show no branchpoint.

Explorer is shown in Figure 11 A. The idea behind analyzing this parameter was, that the more varicosities are present, the more synapses may be present allowing communication with neurons in a given target area. On the contrary, fewer varicosities would indicated less functional communication in the target area. First, I wanted to test, if density of varicosities is a reliable parameter usable to compare the density of axon pieces with different length. For all regions, a highly significant correlation was found in a linear regression model between the amount of varicosities and the axonal length (adjusted $r^2 = 0.918$, $p < 0.001$; Fig. 11 B). Highly significant correlations were also found when analyzing the data from all main target

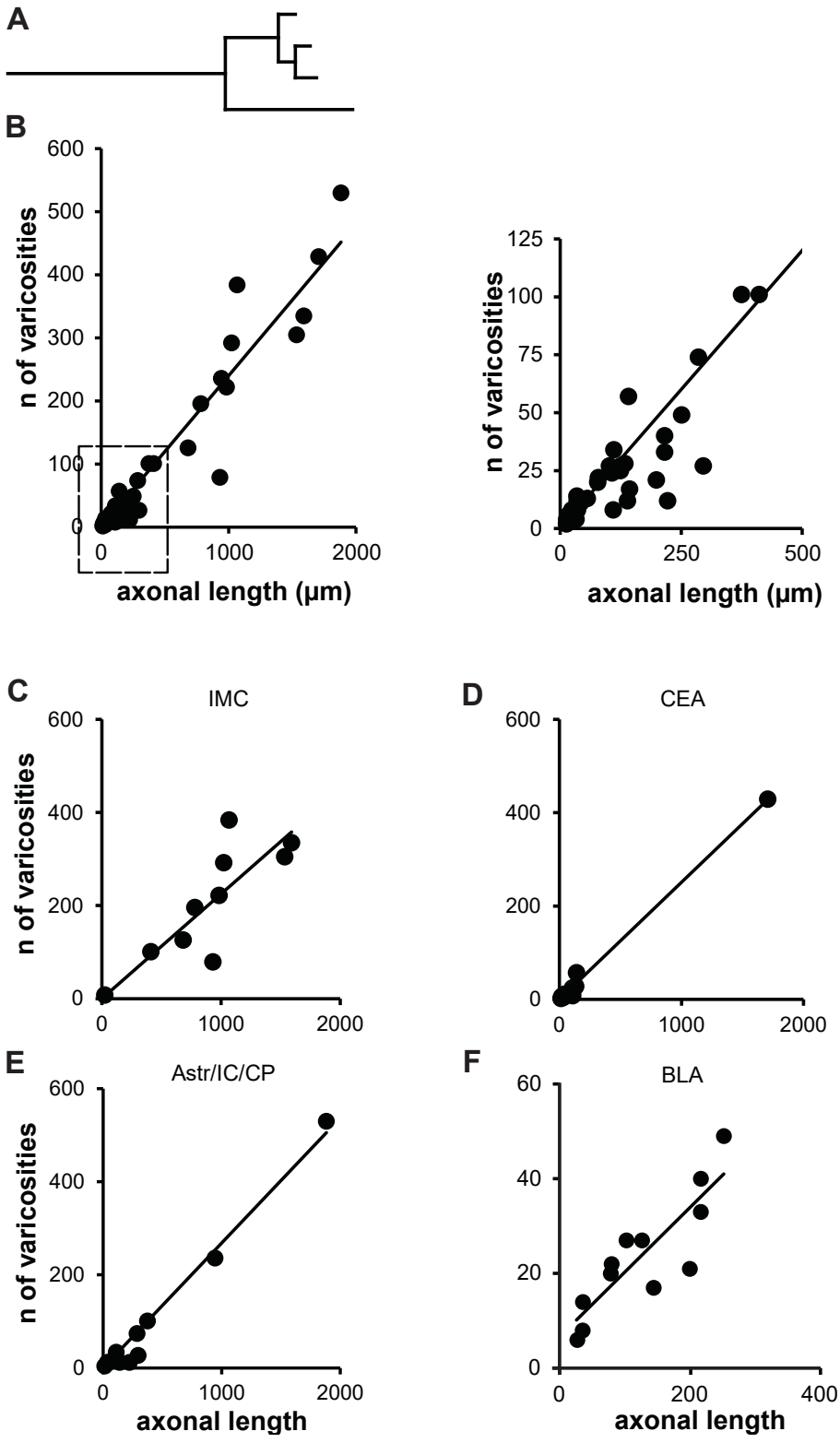

Figure 11: **Axon parameters: Overall varicosity analysis**

Figure 11: Axon parameters: Overall varicosity analysis (to be continued): Scheme of axon (dendrogram) showing branchpoints and varicosities. (B1-B2) Dataset of all n=44 regions targeted by 10 mpITCs. Linear regression analysis shows a significant correlation between number of varicosities and axonal length in all target regions ($F(1,42)=485.536$, $p<0.001$, adj. $r2=0.918$). (B2) Graph is a zoom in of graph B1, indicated by dotted frame. (C) Data for n=10 IMC target regions. Linear regression analysis shows a significant correlation between branch amount of varicosities and axonal length in the IMC target region, $F(1,8)=16.759$, $p=0.003$, adj. $r2=0.636$, slope (s)=0.22 (D) Data for n=11 CEA target regions. Linear regression analysis shows a significant correlation between branch amount of varicosities and axonal length in the CEA target region (grouped CeC, CeL, CeM), $F(1,9)=1534.05$, $p<0.001$, adj. $r2=0.994$; slope (s)=0.25 (E) Data for n=11 Astr target regions. Linear regression analysis shows a highly significant correlation between branch amount of varicosities and axonal length in the Astr target region (grouped with IC and CP), $F(1,9)=475.985$, $p<0.001$, adj. $r2=0.979$; slope (s)= 0.28 (F) Data for n=12 BLA target regions. Linear regression analysis shows a highly significant correlation between branch amount of varicosities and axonal length in the BLA target region (grouped LA and BA), $F(1,10)=28.141$, $p<0.001$, adj. $r2=0.712$; slope (s)=0.14.

regions separately: the IMC, the CEA, the Astr/CP/IC, and the BLA (adjusted $r^2 > 0.7$ for all, $p < 0.002$ for all; Fig. 11 C - F). In contrast to the branchpoint analysis, there were no short axon pieces that lacked varicosities. Therefore, density if varicosities can be used as a reliable parameter to describe axon communication infrastructure. Interestingly, the slope of the regression analysis was nearly identical for all the main target regions (Fig. 11 C-F). This would suggest a similar density of varicosities in all main target regions. To test more directly, if there is a difference between the main target region's average density of varicosities, means of density were compared along the different regions. No significant difference was found between the IMC, CEA, the Astr/CP/IC, and the BLA (OWA, $p > 0.9$; Fig. 12). That indicated that at least in the subset of cells analyzed with Neurolucida, there was currently no evidence for a regional specificity in the density of possible innervation. Therefore, to describe the functional impact of axon communication, axonal length may be an important and sufficient parameter.

In summary, we tested two communication infrastructure parameters, density of branchpoints and density of varicosities, for their usability to describe efferences with higher functional impact. Density of varicosities was identified as a reliable parameter, but so far no differences were seen among the target regions. This indicated no functional specialization of distinct target regions concerning this parameter.

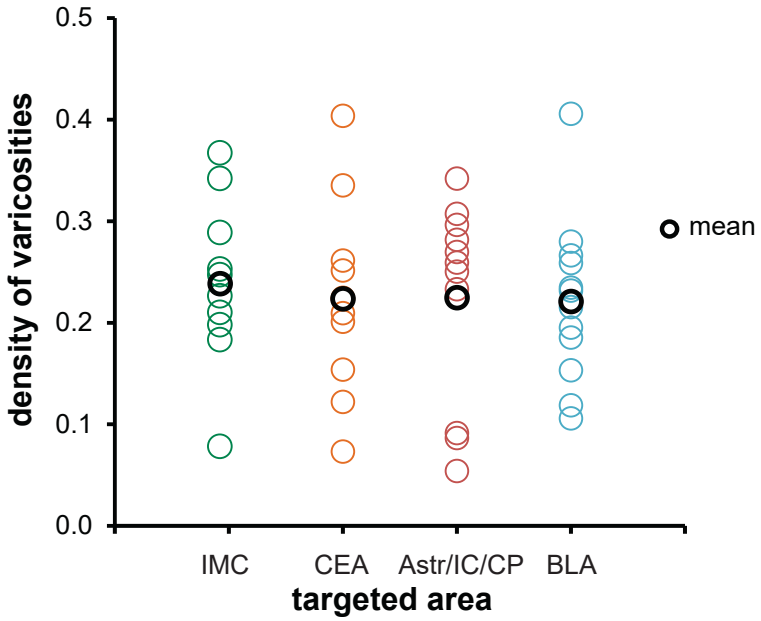

Figure 12: **Similar density of varicosities in all different target regions**
Plot of the density of varicosities in axonal branches by individual target regions from n=10 mpITCs. Average density values (number of varicosities/μm axon) and SEM were: IMC 0.238 $\pm$ 0.025 (n=10), in CEA region (grouped CeC, CeL, CeM) 0.224 $\pm$ 0.028 (n=11) and in Astr (grouped with IC and CP) 0.225 $\pm$ 0.030 (n =11) density values, in BLA region (grouped LA and BLA) 0.221 $\pm$ 0.019 (n=12) density values. Mean indicated by fat circle line. OWA: F(3;40)=0.083, Tukey-HSD post hoc test p>0.9.

3.2.2 Classification of mpITC projection types in adult animals based on axonal length analog to classification in young animals

A further aim was to clarify if mpITCs of young adult animals show different projection types as in young animals (Busti et al., 2011) and as our qualitative analysis suggests. Classification criteria were now based on the precise axonal length in the target regions, analog to classification of mpITCs with unsupervised cluster analysis in young mice (c.f. Busti et al., 2011). Measurements of axonal length show patterns compatible with young animals: Firstly, an IMC projection type is shown, distributing the highest amount of axon locally in the IMC (Fig. 13 C). Secondly, a CEA projection type is shown with the highest amount of axon

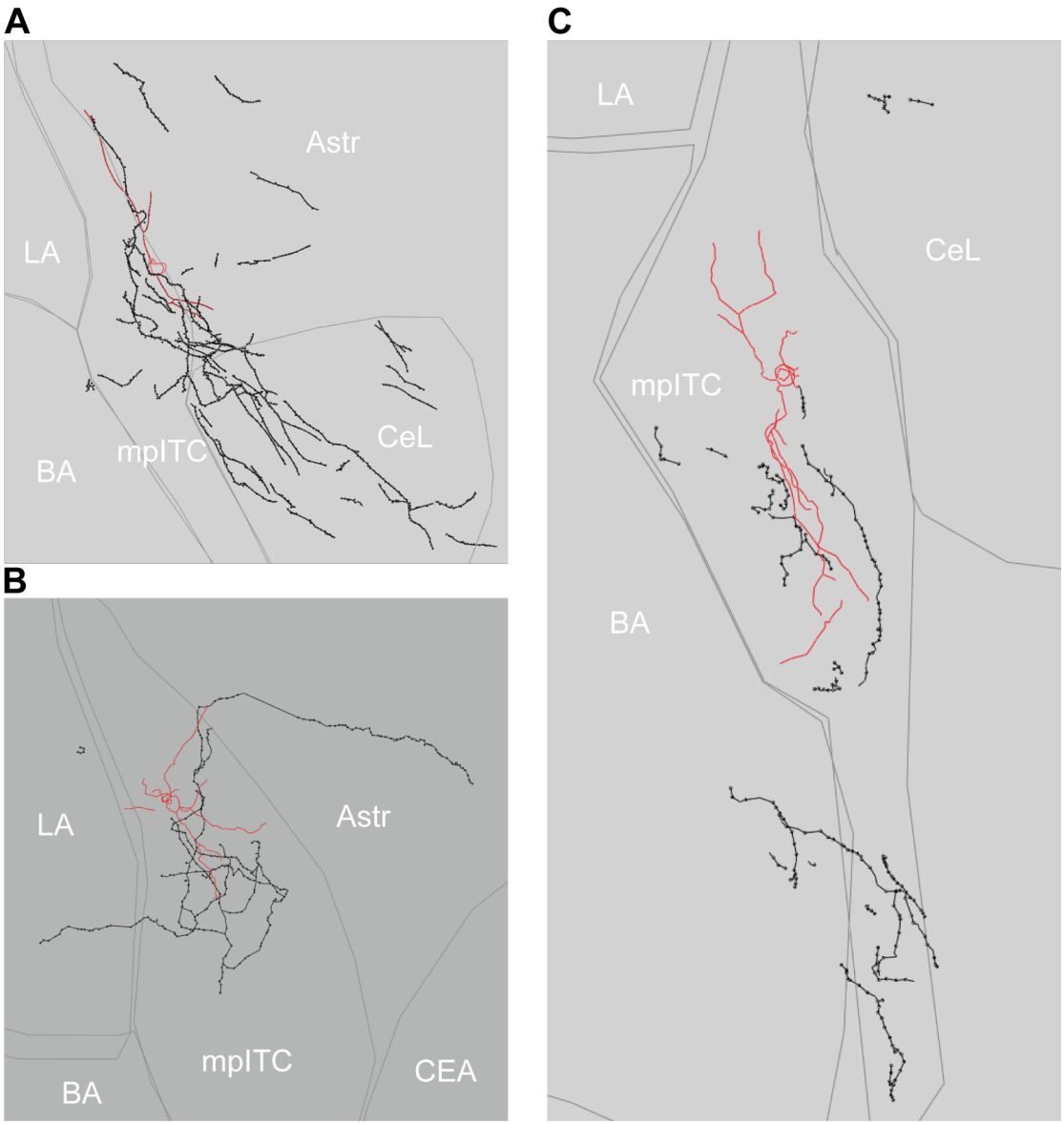

Figure 13: **3D-reconstructed mpITCs illustrating three different projection types**
(A-C) Images of fully 3D reconstructed mpITCs aligned with in the shape of the amygdaloid nuclei obtained from the first sections of coronal slices. Soma and dendrites in red, axon with presynaptic boutons in black (A) Example of an IMC projection type with >90% of axon in the IMC region, total axonal length: 1016.6 μm. (B) Example of an CEA projection type with >50% of axon in the CeL, total axonal length: 3322.8 μm. (C) Example of an Astr projection type with >20% of axon in the Astr region, total axonal length: 1144.6 μm.

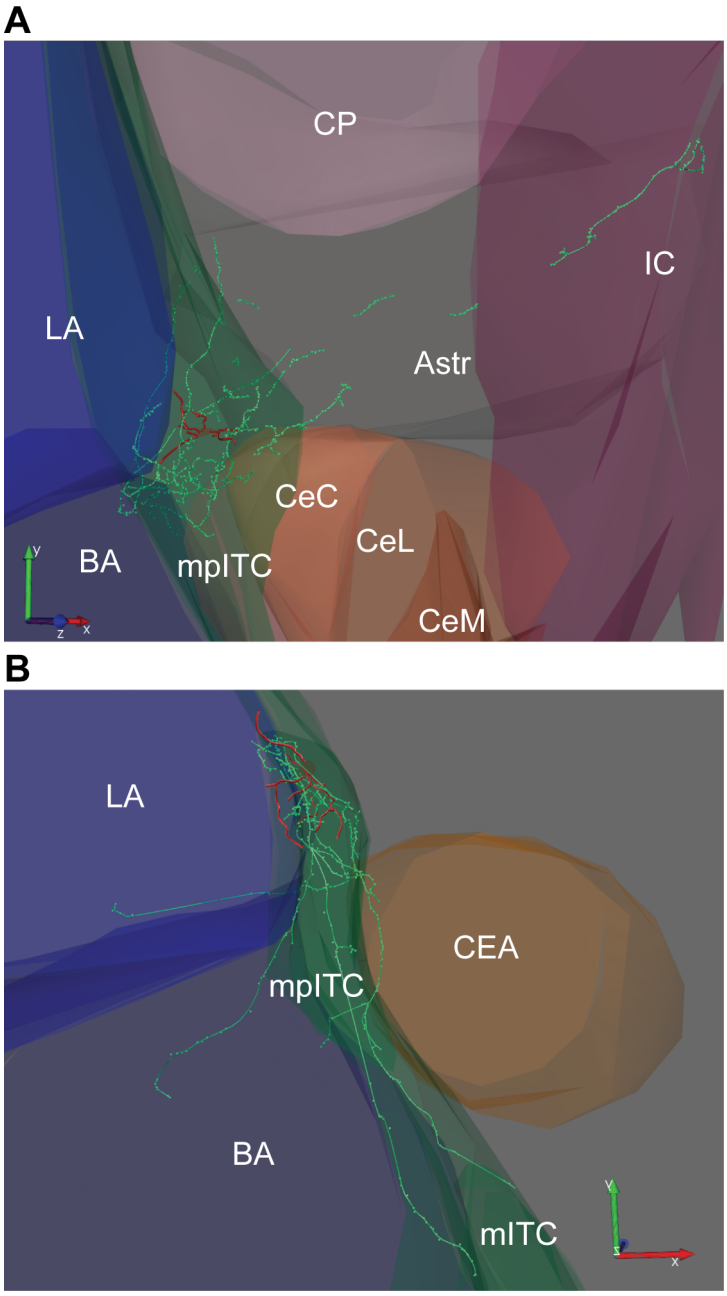

Figure 14: **3D-reconstructed mpITCs and amygdaloid nuclei illustrating two different projection types**

(A-B) Images of fully 3D-reconstructed mpITCs within the shape of fully 3D-reconstructed amygdaloid and adjacent nuclei. Soma and dendrites in red, axon with presynaptic boutons in green. Highlighted are amygdaloid and adjacent nuclei as the BLA (in blue), the CEA (in orange), the Astr (in gray), the CP (in rose), and fiber tracts as the IMC (in green) and the IC (in magenta).

(A) Shown is an Astr projection type, reconstructed and in slice spliced, with more than 30% amount of axon in the Astr region, total axonal length: 2916.8 μm. (B) Shown is an BLA projection type, reconstructed and fully spliced, with more than 20% amount of axon in the BLA region, total axonal length: 2168.4 μm.

traveling to the CeL (Fig. 13 B). Thirdly, two Astr projection types are shown with the highest amount of axon in the IMC, followed from Astr (Fig. 13 A and 14 A). Additionally, BLA projection types are present, which have not been reported in young animals, but were recently observed in adult animals in our group (Asede et al., 2015). This type shows the highest amount of axon in the IMC, followed by a substantial amount of axon in the BLA (Fig. 14 B). All classified cells with their different proportion of axonal length in distinct target areas are shown in Fig. 15. The distribution of average axonal length in distinct target regions for IMC-, Astr-, and CEA-projecting types in young adult mice looked largely compatible with the medial capsular-projecting (MCp) neurons preferentially targeting the IMC, sublenticular-projecting (SLp) neurons preverentially targeting the Astr or AL, and central-projecting (Cp) neurons preverentially targeting the CEA found in young animals (Fig. 15 B). However, some differences existed: Adult animals showed a much higher proportion of projections to the Astr and BLA over all projection types. For the cells classified as Astr-projecting types, the average proportion was almost twice as high. In young adult animals, some mpITCs preferentially targeted the BLA with an average proportion of $> 20\%$ of axon in this region (c.f. Asede et al., 2015). On the contrary, a much lower proportion of projections to the CeL was seen over all projection types. Also the cell classified as CEA-projecting type showed a lower proportion of axonal length there (Fig. 15 B_{right}). My findings suggested that different projection types exist in adult animals even though more mature mpITCs showed a different composition in the axonal length proportions in some target areas and an additional BLA-projecting (BLA-p) type. Interestingly, among these classifiable cells in adult animals, we observed some cells with their axonal distribution pattern at the edge of fitting into one of the projection types. These cells showed among each other a somehow similar distribution of axonal amount with axon in the IMC plus substantial amount of axon in at least two other major target regions. An example of such a cell, classified as Astr projection type, but showing as well a substantial amount in the LA is shown in Figure 13 B.

Taken together, my results supported the idea of different mpITC projection types to the IMC, the Astr, the CEA, and the BLA. At the same time, these results brought up the question, if there is a smooth continuum between the different projection types or if some cells are part of a separate additional group of mpITC projecting to mainly at least three target regions.

A

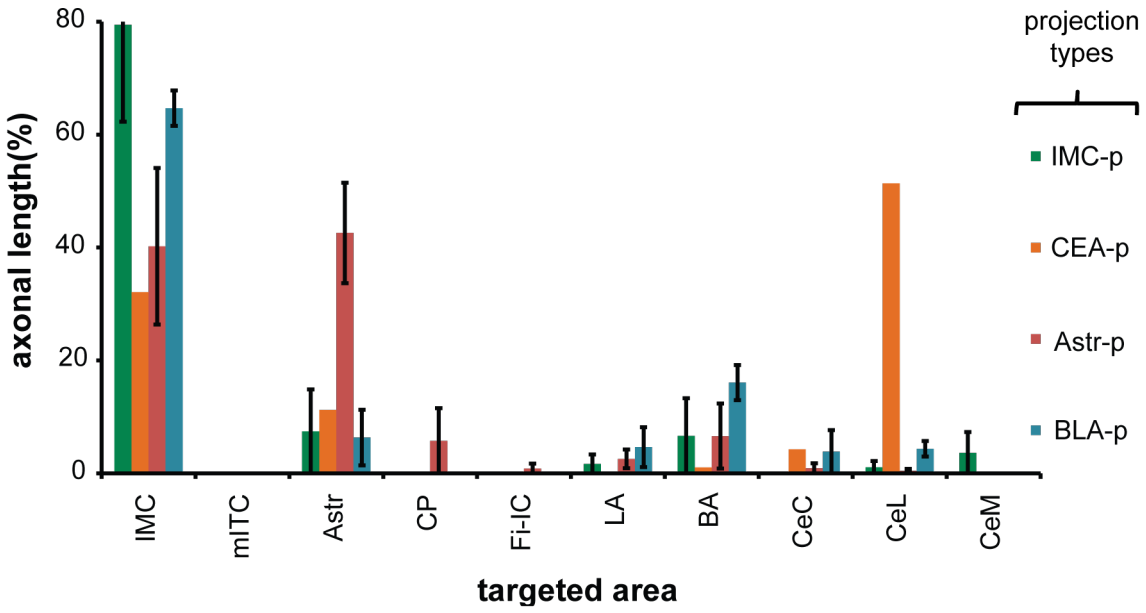

B

	young mice (15-25 days)			young adult mice (6-10 weeks)			
main target areas	distribution of axonal length (%) in different projection types						
	MCp	SLp	Cp	IMC-p	Astr-p	CEA-p	BLA-p
IMC	**90**	50	18	**80**	40	32	65
Astr + AL	< 1	**17 + 7**	4 + 3	7	**40**	11	6
CeL	4	25	**65**	1	< 1	**51**	4
BLA	4	3	2	9	10	1	**21**

Figure 15: **Summary of axonal contributions to different target region among mpITC projection types**

(A) Graph comparing the relative contributions of the overall axon (in %) to projections into distinct target regions for the different projection types (n=10 cells from Neurolucida reconstructions). IMC projection types in green, CEA projection type in orange, Astr projection type in magenta, BLA projection type in blue. Error bars indicate SEM. (B) Comparison between young mice (results adapt. f. Busti et al., 2011) and young adult mice for the distribution of average axonal length (%) in different projection types. Numbers are rounded to no decimal place. Listed are: (B_{left}) Target areas IMC, CeL, Astr (grouped with AL only for young mice), and the BLA. Simpified as only main target areas are listed. (B_{middle}results adapt. f. Busti et al., 2011) The three different projection types classified by unsupervised cluster analysis in young mice: Medial capsular projecting (MC-p) cells (n=17), sublenticular projecting (SL-p) neurons (n=16), projecting to the Astr and AL, and CEA projecting (C-p) neurons (n=18) with their proportion of average axonal length (%) in target areas. (B_{right})The four different projection types classified analog to the ones found in young mice: IMC-projecting mpITCs (n=2), Astr-projecting mpITCs (n=4), CEA-projecting mpITCs (n=1), BLA projecting neurons (n=3) with their proportion of average axonal length in target areas.

3.3 Immunohistochemical identification of putative postsynaptic partners of mpITCs in target regions

In this part, the aim was to identify putative postsynaptic partners of mpITCs by labeling specific neuron types present in the axonal target regions. The target regions that were investigated were the IMC, CEA and Astr. As staining of L-ITCs using the markers mGluR 1α and NK-1 located in the periphery of the mpITC cluster did not work in a stable manner, no results will be described for IMC, and I will focus on CEA and Astr.

3.3.1 Identification of putative contacts of mpITC axon on PKC δ^+ and SOM$^+$ cells in the central nucleus

As it is known that the CeL contains two functionally opposing cell types (Haubensak et al., 2010; Li et al., 2013) and that mpITC synapse onto cells in CeL (Busti et al., 2011), the next step was to identify which of these cell populations may receive putative synapses. This may help to define the putative function of CEA-projecting mpITCs. Using immunohistochemial markers for PKC δ and SOM in coronal amygdala slices (Fig. 16 A and 17 A), I confirmed that labeling of PKC δ^+ cells was restricted to the CeL (Fig. 16 A) and that labeling for SOM$^+$ cells was seen in the CeC/CeL (Fig. 17 A). Subsequently, applying these markers in slices containing fluorescently labeled mpITC axon in the CEA, I wanted to identify putative synaptic contacts between them using confocal microscopy (Fig. 16 B and 17 B). Firstly, in one out of three PKC δ-labeled slices, a close proximity between an mpITC axonal varicosity and PKC δ^+ soma in the CeL was identified (Fig. 16 C), indicating that mpITCs could target somata of PKC δ^+ cells. Secondly, in one out of ten SOM-labeled slices, I found a close proximity of an mpITC axonal varicosity and a thick, SOM$^+$ proximal dendrite (Fig. 17 C), suggesting that mpITCs could also target SOM$^+$ cells in CeC.

So far, my results provided preliminary evidence that mpITCs could contact two functionally opposing neuron types in the CeC/CeL. Interestingly, the putative contacts were located in strategic positions to control neural output via GABAergic synapses, i.e. the soma and proximal dendrite of target cells.

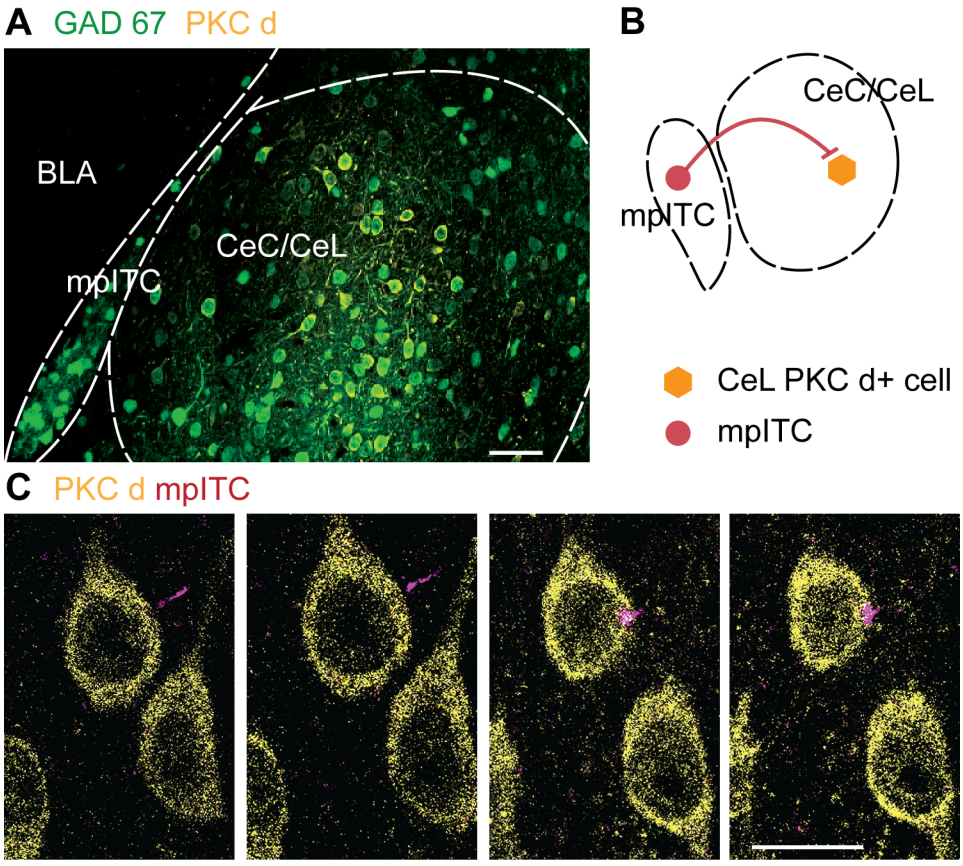

Figure 16: **MpITC axon makes putative contact on PKC δ^+ CeL soma**
(A) Confocal image of coronal amygdala slice of GAD67-GFP mouse with immunohistochemical labeling for PKC δ restricted to a subpopulation of CeL GABAergic neurons. GABAergic neurons contain GAD67 labeled by GFP, PKC δ^+ cells are shown in yellow. Scale bar: 50 μm. Dotted line denotes the borders of BLA, mpITC cluster and CeC/CeL. (B) Scheme of mpITC with inhibitory synapse on PKC δ^+ CeL cell. (C) Consecutive z-sections (0.5 μm) of confocal stack showing Cy3 labeled mpITC axon with presynaptic varicosity on PKC δ^+ soma in CeL. Axon is shown in magenta, PKC δ^+ cell in yellow. Scale bar: 10 μm.

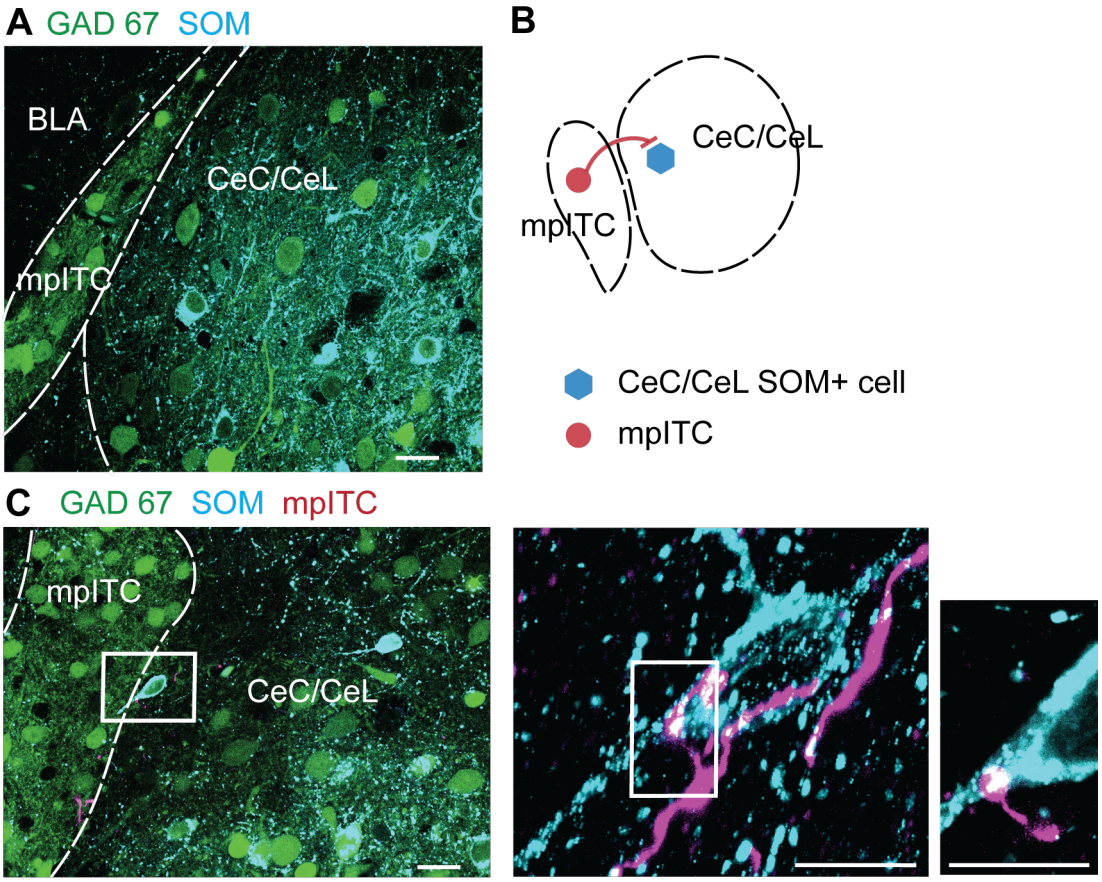

Figure 17: **MpITC axon makes putative contact on SOM$^+$ CeC/CeL proximal dendrite**
(A) Confocal image of coronal amygdala slice of GAD67-GFP mouse with immunohistochemical labeling of SOM$^+$ neurons in the CEA. GABAergic neurons contain GAD67 labeled by GFP, SOM$^+$cells are shown in turquoise. Scale bar: 20 μm. Dotted line denotes the borders of BLA, mpITC cluster and CEA. (B) Scheme of mpITC with inhibitory synapse on SOM$^+$ CeC/CeL cell. (C_{left}) Confocal image of coronal amygdala slice of GAD67-GFP mouse with Cy5 labeled mpITC axon (magenta) and immunohistochemical labeling of SOM$^+$ neurons in the CeC/CeL (turquoise). Scale bar: 20 μm. Dotted line denotes the border of mpITC cluster and CeC/CeC. ($C_{middle\ and\ right}$) Magnification of white rectangle in C_{left} showing mpITC axon (magenta) with axonal varicosity on SOM$^+$ proximal dendrite (turquoise). Scale bar: 10 μm. (C_{middle}) Z-section from confocal stack, thickness 0.5 μm. (C_{right}) Magnification of putative synaptic contact.

3.3.2 MpITC axon closely passes cholinergic proximal dendrite in the amygdalo-striatal transition zone

The Astr is comprised of different types of interneurons, among them cholinergic ones as in other striatal regions. They are reported to have large somata compared to other interneurons found in the striatal area (Tepper & Bolam, 2004). Staining with the immunohistochemical marker for ChAT in amygdala coronal slices was found in accordance with this (Fig. 18 A and C). To assess if mpITCs with axon in the Astr, contact cholinergic cells in this region, I searched for putative contacts between mpITC axons and ChAT-positive ($ChAT^+$) cells in slices containing Astr-projecting mpITCs (Fig. 18 B). In two out of four slices, mpITC axons were found in close proximity, but appear to be passing $ChAT^+$ proximal dendrites without showing any axonal varicositiy in the overlapping region (Fig. 18 C).

Thus, my results indicated, that while mpITC axons closely passed dendrites of cholinergic cells, it is unlikely that they make contacts as presynaptic varicosities were lacking close to Astr $ChAT^+$ cells.

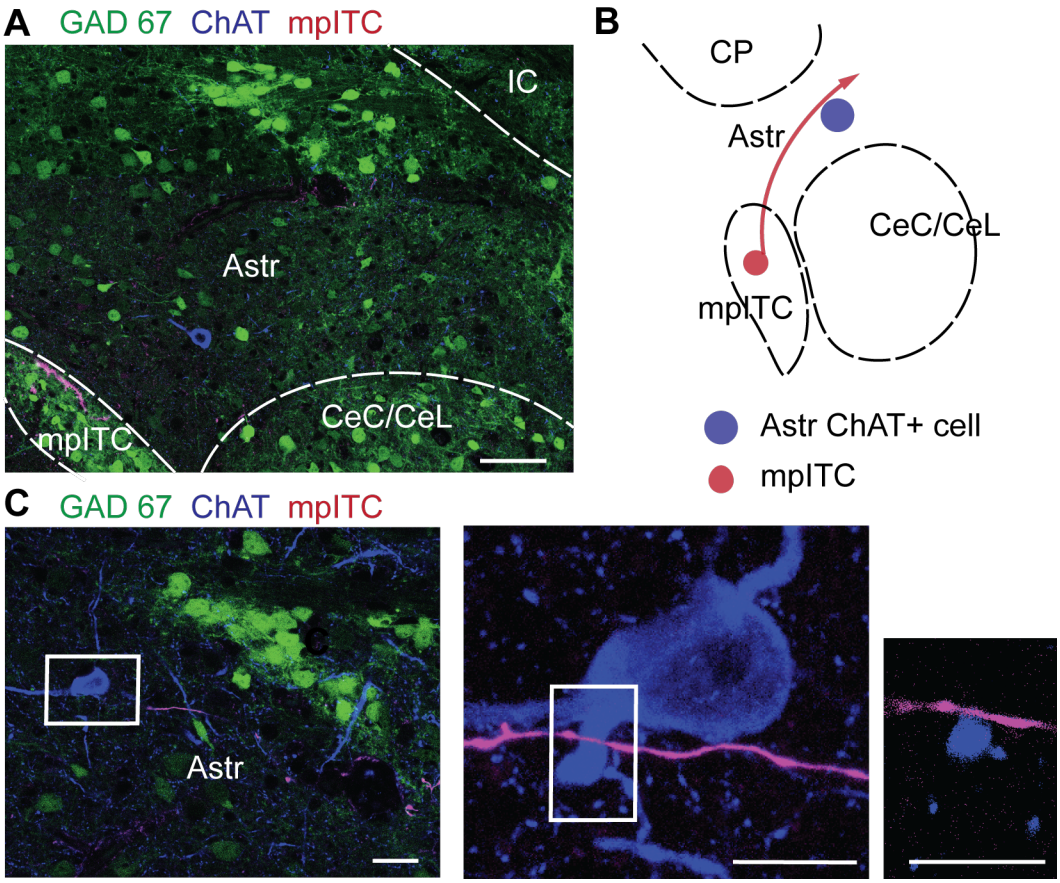

Figure 18: **MpITC axon closely passes cholinergic proximal dendrite in the Astr**
(A) Confocal image of coronal amygdala slice of GAD67-GFP mouse with immunohistochemical labeling of ChAT$^+$ interneurons in the Astr. GABAergic neurons contain GAD67 labeled by GFP, ChAT$^+$ cell is shown in dark blue. Scale bar: 50 μm. Dotted line denotes the borders of mpITC cluster, CEA, Astr and, IC. (B) Scheme of mpITC axon passing cholinergic cell in the Astr. (C_{left}) Confocal image of coronal amygdala slice of GAD67-GFP mouse with labeled mpITC axon (magenta) and immunohistochemical labeling of ChAT$^+$ IN in the Astr (dark blue). Scale bar: 20 μm. ($C_{middle\ and\ right}$) Magnification of area of white rectangle in C_{left} showing mpITC axon passing closely a ChAT$^+$ proximal dendrite. Scale bar: 10 μm. (C_{middle}) Z-section from confocal stack, thickness of 0.5 μm. (C_{right}) Magnification of closest proximity containing z-level from C_{middle}.

4 Discussion

4.1 Heterogeneity of adult mpITC projection patterns

MpITCs have been thought to exert their principal role as inhibitory gate between the BLA and CEA to control fear output of the amygdala (Royer et al., 1999; Pape & Pare, 2010). Studies in young animals started to reveal that mpITCs can participate in additional intra- and extra-amygdala microcircuits (Geracitano et al., 2007; Amir et al., 2011; Busti et al., 2011). This is the first study of mpITC output in adult mice. Our qualitative analysis confirms that projection patterns, seen in young mice (Bienvenu et al., 2012), are also present in the adult. Because all cells have local axons in the IMC, the previously reported involvement of all cells in an intracluster network (Geracitano et al., 2007) seems highly plausible. As more than half of all randomly filled cells show axon collaterals in the Astr, it is likely that mpITCs can also control Astr networks. Only a quarter of cells sends some axon collaterals in the CEA, confirming this as a known site that is impacted by mpITCs, but it does not appear to be the major output. Furthermore this study provides first evidence that mpITCs target previously not reported projection sites. A quarter of cells disperses axon collaterals in the BLA. This indicates that an unexpectedly high proportion of cells is targeting this area which could exert feedforward and feedback inhibition to effectively control this nucleus (Asede et al., 2015). We found rare cells with axon traveling to the MEA, suggesting a minor impact of mpITCs in this nucleus. Axon traveling through the Astr and continuing to the CP or the IC were seen in few cells, indicating that cells with Astr axon may exert different roles depending on the final destination of their axon. Our qualitative analysis of the projection pattern reveals that mpITCs project to at least two target regions, one of which is always the IMC, and usually, the second one is one that is preferentially or more strongly targeted. Thus, on a single cell level, mpITCs seem to exert at least a double role. Some mpITCs disperse axons even into up to six other target regions, creating a more general output. Overall, since cells with different target areas are intermixed in the cluster and present at different bregma levels, this could indicate that the mpITCs as a group could influence several targeted areas in parallel. Analysis of the whole mpITC cluster output is also in line with this, as it revealed a heterogeneous output that remained similar along the rostro-caudal axis. Although two distinct ITC clusters were reported in the IMC by Busti and colleagues (Busti et al., 2011), my data suggests that they are similar regarding their anatomical output. The dataset with a large number of neurons (119 cells) and the random selection of mpITCs is a good basis to obtain a first representation of the cluster's projection distribution.

4.2 Axonal parameters to characterize output of adult mpITCs and evidence for different projection types

Describing anatomy-based parameters for communication infrastructure of mpITCs axons can give first insights into the function of the output. Here, I assessed axonal length in different areas as well as branchpoints and varicosities. Concerning branchpoints, a strong correlation with axonal length indicates that the longer the axon is in a targeted area, the more local wiring and communication could takes place there. However, because there was also a substantial fraction of axons <300 μm without any branchpoint, it is not straight forward to interpret the data from this analysis. Concerning the number of varicosities, my results again indicate that this parameter is tightly correlated with axonal length in all the observed target regions. Thus, the longer the axon is in a given area, the more varicosities are present, providing a substrate for more functional axonal output. Furthermore, the average density of varicosities was similar in all target regions. Together, this suggests that the axonal length in different target regions seems sufficient to characterize the impact on a target region and to identify the different specialized projection types of mpITCs. However, other communication infrastructure parameters, not analyzed in this study, could be the distribution of distances in between varicosities along the axon in a distinct target region to determine if the output occurs in a clustered manner. Or, as we have 3D-reconstructed cells, another parameter could be the 3D arrangement and proximity of putative presynaptic boutons, irrespectively if they are on the same axon piece or on different ones.

My data suggests that individual mpITCs in young adult animals have similarly specialized output as young mice. At the same time, results indicate that there exists a subset of cells with a composition of three main projections, one of which is always the IMC. That allows us to ask if these cells still belong to the range of classified projection types or may represent an additional, more complex type. With our first attempt at classification with a low n number (10 cells), it is not possible so far to answer this question. Additionally the subset of cells analyzed with Neurolucida is a non-random selection, as these cells have been qualitatively analyzed before. An unsupervised cluster analysis, which requires a higher n-number is needed to strengthen our results and to distinguish if the transition between the different projection types is smoother in adult compared to young animals, or if there are differently specialized adult mpITCs that show a higher complexity in addition to those that are specialized in influencing mainly one target region apart from IMC.

In general, working with reconstructed DAB-converted cells and surrounding nuclei, always

needs to be interpreted with the knowledge about the subjective nature of reconstructing with Neurolucida software. This limitation can be overcome by working tightly with the brain atlas and available images from the fluorescent and confocal microscope.

4.3 General methodological constraints of in slice - cell reconstruction

In general, analysis of filled cells in slices is always limited because axons are most likely cut off during slicing progress, leading to an underestimation of axonal trajectories. These limitations can only be overcome by reconstruction of in vivo-filled cells. The differences in the heterogeneity of mpITC projections or the fact that I find a much smaller fraction of CEA projections and a larger of Astr projections in adult animals as previously reported in young ones (Geracitano et al., 2007; Busti et al., 2011) lack tight explanation. On the one hand, this could be a developmental difference, but currently, no data are available on the axonal development of GABAergic cells in the amygdala in mice. On the other hand, the differences could be in part methodological, due to slight differences in the cutting axis and filling of cells as well as to the use of a slightly different mouse line. Certainly, the question of how the efferent projection pattern of these cells looks like in the whole brain would be an interesting task for future studies.

4.4 Putative postsynaptic partners of mpITCs

The mpITCs axons have presynaptic boutons in a variety of target areas, including those revealed in a previous study, indicating that they make synapses with other ITCs in the IMC clusters, the Astr and, the CeC and CeL (Busti et al., 2011). Here, identification of target cells in Astr and CeC/ CeL was attempted.

In the Astria, mpITC axons just appear to pass cholinergic dendrites, indicating that it is unlikely that they modulate cholinergic tone locally in the Astr. However, as some cells pass the Astr and continue to fiber bundles of the IC, it would be interesting to see in future experiments, if axons continuing to to the basal forebrain associated areas could modulate cholinergic tone via this trajectory. Indeed, other amygdaloid nuclei are reported to modulate cholinergic tone (Shammah-Lagnado et al., 1999; Jolkkonen et al., 2002). Another aim for the future could be to identify if mpITCs may contact other interneurons present in the Astr.

In the CeL, an mpITC axon makes a putative contact on a PKC δ^+ cell body. The strategic somatic location of this putative contact could exert efficient control on the PKC δ^+ cell's

firing pattern. Moreover, the cell making this putative contact seems to be specialized in inhibiting PKC δ^+ cells as its axon was mainly restricted to the IMC and the CEA (Fig. 4 D and Fig. 16 C), and did not show putative contacts with the other major population of SOM$^+$ cells in the CeC/CeL. PKC δ^+ cells are so called Fear$_{OFF}$ cells in CEA microcircuits (Ciocchi et al., 2010; Haubensak et al., 2010) and their inhibition could result in disinhibition of CeM, the main amygdala output (Fig. 19).

In the CeC, an mpITC axon also makes a putative contact onto the proximal dendrite of a SOM$^+$ cell (Fig. 17 C), and thereby could exert efficient control of the cell's activity. This mpITC sends also a major branch to the BLA and one coursing through the CEA to reach the Astr region (Fig. 4 A), indicating that it distributes its inhibitory impact on several regions. SOM$^+$ cells are so called Fear$_{ON}$ cells in CEA microcircuits (Ciocchi et al., 2010; Haubensak et al., 2010; Li et al., 2013) and their inhibition could result in an reduced signal transfer of CeL-SOM$^+$ long range projections or in inhibition of CeM output (Fig. 19).

Overall, identification of putative postsynaptic partners of mpITCs in Astr, CeC and CeL gives a first impression about mpITCs' possible function in these regions. As the number of observations is low, the results are still preliminary. While a positive finding provides some evidence that connections exist, a negative finding does not yet allow me to rule out that there is no connectivity. Furthermore, my findings do not provide answers about preferential innervation. A limitations is also that I only used appositions of mpITC presynaptic boutons and target structures as indicator for putative synaptic contacts. Co-staining with Gephyrin as a marker of GABAergic postsynapses would have been useful to support that postsynaptic elements exist at appositions ($< 0.5\ \mu$m) of synaptic boutons with postsynaptic cell structures. However, I did not have a working antibody in an appropriate host species at hand to do these experiments. In the future, immuno-electron microscopy, viral tracing and functional investigations are needed to further strengthen these findings.

4.5 Possible impact of mpITC activity in distinct target regions

As I have highlighted the heterogeneous projection pattern of mpITCs including the IMC, CEA, Astr, CP, IC, BLA and the MEA, I will discuss the possible functional impact of mpITCs activity in the distinct target regions (Fig. 19).

IMC. MpITCs have been described to have axon collaterals in the IMC (Millhouse, 1986; Royer et al., 1999; Geracitano et al., 2007; Busti et al., 2011) and my findings are in accordance with mpITC interconnectivity. In young animals they provide mainly unidirectional

connectivity. This intra mpITC network uses different modes of short-term plasticity (facilitating, depressing, constant transmission), a property that is determined by the presynaptic neuron. This is thought to maintain the stability of the cluster's output in terms of firing pattern (Geracitano et al., 2007). In almost all cases, mpITCs project to one or more additional target regions. The local network properties could therefore provide stability of firing patterns for information transfer to the other target regions, too. A goal for further studies could be to elucidate if different types of local network neurons are distributed equally over mpITC projection types or if there is a certain correlation between responding and projection types. Also it remains to be determined if the different types of synaptic transmission reported in young animals (Geracitano et al., 2007), are maintained over development.

About 15% of cells exhibit axons that continue to the main cluster (mITC), where they show functional inhibitory synapses in young animals (Busti et al., 2011). Further on, mITCs are known to project to the CeM (Mańko et al., 2011; Blaesse et al., 2015), which may constitute a pathway by which mpITCs can participate in disinhibiting CeM, the main amygdala output.

CEA. Projections to the CEA have been reported in several studies (Millhouse, 1986; Royer et al., 1999; Geracitano et al., 2007; Busti et al., 2011). Additionally, Busti and colleagues confirmed mpITC axon synapses on cells in the CeC and the CeL with electron microscopy. In this thesis, I show that a quarter of all randomly filled cells sends some axon collaterals to the CEA, but only 8% are characterized as CEA-proejcting types, with their major arborizations in the CeC and CeL subdivisions. Our data about putative postsynaptic partners reveals that mpITCs have putative contacts on both major populations in the CeC/CeL. With functional opposing roles of these two putative partners of mpITCs in the CeC/CeL, the role of specific mpITCs seems to be defined by their postsynaptic partner.

Astr. Projections to this area and a subset reaching the adjacent AL have been described in young animals (Busti et al., 2011). I find that more than 60% of all investigated cells project to the Astr and that 30% of all cells are classified as Astr-projecting types. As this is a large fraction, it will be of importance to reveal mpITCs' functional impact there. One idea is, that Astr-projecting axons travel to the AL, as reported in young animals (Busti et al., 2011), as well as other parts of the basal forebrain to modulate cholinergic tone as do other amygdaloid nuclei (Shammah-Lagnado et al., 1999; Jolkkonen et al., 2002). Another idea is that these axons participate in autonomous regulation via projections to the IPAC, as this region is implicated in regulating parameters associated with the autonomous nervous system such as arterial blood pressure (Krémarik et al., 1995).

Caudate Putamen. Axons of a few mpITCs travel through the Astr to reach the ventral tip of

the caudate putamen, and these projections have not clearly been reported before. The CP, which is part of the striatum, harbors cells which differ in expression of receptors, as well as released neurotransmitter and neuromodulators (Bolam et al., 2000). Clearly, further studies are required to assess functional consequences of this projections.

Internal Capsule. The IC is another novel region in which mpITCs axons were found. Only few cells show axon collaterals that reach the internal capsule at the medio-dorsal tip of the Astr. These axon collaterals show presynaptic boutons there and it would be interesting to investigate if functional synapses exist, and their postsynaptic partners there. As the IC is a major fiber tract that contains up- and downstream fibers (Canty & Murphy, 2008; Leyva-Díaz & López-Bendito, 2013), additional studies could reveal if axons continue further dorsally along the IC to reach the fimbria of the hippocampus (c.f. Franklin & George Paxinos, 2008), containing hippocampal afferences.

BLA. Projections to this area have recently been reported and functionally confirmed in our lab (Asede et al., 2015). The qualitative analysis of the large dataset reveals that more than 30% of cells have axon collaterals in the BLA, and 14% are characterized as BLA projection types. Contrary to the canonical view that mpITCs only receive information from BLA (Paré et al., 2004), these cells make synaptic contacts on distal dendrites of BLA principle neurons, participate in feedback inhibition and thereby efficiently control the output of the BLA (Asede et al., 2015). As BLA projecting cells on average target three areas, it would be interesting to reveal if they constantly target a specific region additional to the IMC and the BLA.

MEA. Out of 39 cells, only one cell was found with axons traveling along the IMC and then ventral of the CEA towards the bed nucleus of the Stria terminalis and the medial extended amygdala. Nevertheless, it would be interesting to reveal in further studies if mpITCs have an impact on these regions implicated more in sustained fear and anxiety (Davis et al., 2010).

4.6 Relevance in amygdala circuits of high and low fear

MpITCs were previously thought to participate in the control of fear by providing mainly an inhibitory gate between the sensory input receiving BLA and the physiological fear response triggering CEA (Royer et al., 1999; Paré et al., 2004; Jüngling et al., 2008). Thereby, they were thought to mainly inhibit fear (Pape & Pare, 2010) and play a central role in fear extinction (Likhtik et al., 2008). Our and other recent results indicate that an update of this model is required: Firstly, mpITCs also receive direct sensory input in addition to BLA projections (Asede et al., 2015; Strobel et al., 2015), and BLA inputs are under tight neuromod-

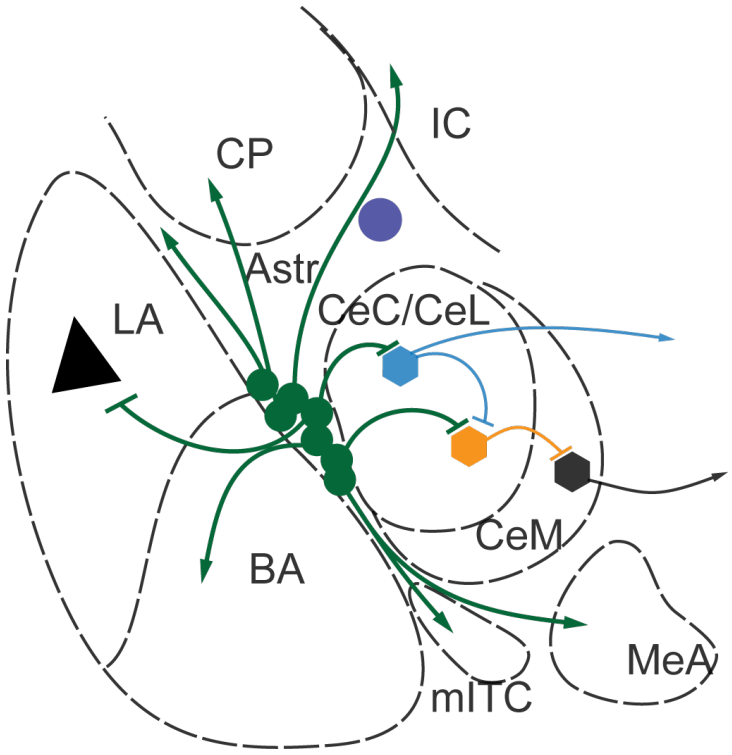

Figure 19: **Model of mpITC efferent connectivity and relevance in states of high and low fear** Heterogeneity of mpITC projection patterns with connections in the IMC, to the Astr, the CP and the IC, the CEA and to BLA and MEA. Putative postsynaptic partners of mpITCs in CEA sub nuclei and an mpITC axon passing a $ChAT^+$ Astr cell are indicated. MpITCs inhibitory synapses on SOM^+ $Fear_{ON}$ cells, may reduce high fear states, whereas synapses onto PKC δ^+ $Fear_{OFF}$ cells, may increase fear behavior. Color code: mpITC cluster in green, $ChAT^+$ cell in dark blue, SOM^+ cell in light blue, PKC δ^+ cell in yellow and CeM neurons in black. Model adapted from Duvarci & Pare, 2014, Asede et al., 2015, and providing own results.

ulatory control (Jüngling et al., 2008; Palomares-Castillo et al., 2012). Secondly, the output of mpITCs exhibits a large diversity beyond targeting CEA (Fig. 19), which is in accordance and expands former findings (Busti et al., 2011; Geracitano et al., 2007), suggesting different functions. Our results about the complexity of projection patterns and the idea that there exist different projection types suggest that there may be cells specialized in modulating states of high and low fear by inhibiting postsynaptic partners in different target areas. This hypothesis may be supported by findings of immediate early gene mapping studies, where subsets of cells, but never the whole cluster become active after different behavioral paradigms that induce high or low fear (Hefner et al., 2008; Knapska & Maren, 2009; Whittle et al., 2010; Busti et al., 2011). In this context, it would be very interesting to combine tracing studies with immediate early gene mapping to identify the specific projection types that are activated by opposing fear states (c.f. Senn et al., 2014).

Possible involvement in high fear states. Synaptic connections of CEA projecting mpITCs onto $fear_{OFF}$ cells in the CeL (Ciocchi et al., 2010; Haubensak et al., 2010) suggest that once activated, this group of mpITCs can promote states of high fear (Fig. 19). In accordance with that, some mpITCs show zif268 labeling after fear conditioning (Busti et al., 2011) and receive the needed sensory input either directly or via the LA (Duvarci & Pare, 2014; Huang et al., 2014; Asede et al., 2015; Strobel et al., 2015). Another pathway leading to an increased fear output is via an inhibition of mITCs resulting in disinhibition of the CeM (Busti et al., 2011; Blaesse et al., 2015).

Possible involvement in low fear states. Our qualitative data shows that there exist cells projecting to both, the CEA and the BLA. In the CEA, an mpITC axon shows a putative contact on a SOM^+ cell. These SOM^+ cells comprise a neuron population crucial to drive fear responses (Li et al., 2013), so called $Fear_{ON}$ cells (Haubensak et al., 2010; Duvarci & Pare, 2014). Thus these mpITCs could promote states of low fear by inhibiting $Fear_{ON}$ cells (Fig. 19). Concurrent, mpITCs were shown to make inhibitory contacts on BLA PNs' distal dendrites (Asede et al., 2015). This distributed inhibition to CEA and BLA could be important to inhibit the fear activated LA-SOM^+pathway (Li et al., 2013; Penzo et al., 2015, 2014). Strengthening this hypothesis, mpITCs are shown to be active during fear extinction learning (Busti et al., 2011).

Taken together, first insights are provided into the heterogeneity of mpITC output in adult mice. My data together with recent literature suggest that there are possibly specialized groups of mpITCs in regulating both, states of high and low fear in parallel pathways. Still,

further investigations are needed to strengthen the models provided here: 1) A more complete dataset of quantitative mpITC output is needed to strengthen morphological characterization of projection types. 2) A more quantitative assessment of mpITC connectivity on functionally opposing CeC/CeL neurons is needed and to which projection types they belong. 3) The identification of mpITC postsynaptic partners in other target areas is of high interest, especially for the pronounced local interactions with Astr and for long-range axons to CP, the AL or, the IC. 4) To understand mpITCs role in different fear states, functional investigations would be needed to assess mpITC recruitment during states of high and low fear and the strengthening and weakening of their connectivity during behavioral training.

5 Summary

The amygdala plays a crucial role in the processing of fear and anxiety and in related disorders. It is situated in the temporal lobe and consists of several distinct nuclei that receive sensory inputs and project to downstream regions that mediate behavioral responses associated with fear. Whereas the role of glutamatergic projection neurons has been thoroughly investigated, the function of amygdala GABAergic networks is incompletely understood. GABAergic neurons are thought to modulate fear processing via inhibition and disinhibition. Part of the inhibitory network is, composed of distinct clusters of small GABAergic neurons, the intercalated cells (ITC), situated along fiber tracts surrounding the basolateral complex. Current evidence suggest that medial paracapsular ITCs (mpITCs) modulate fear processing, as they are active in fear and extinction learning, and their ablation impairs extinction memory retrieval. In addition, recent findings suggest that these cells exhibit heterogeneous projection patterns. Therefore, investigation of their anatomical projection patterns and postsynaptic targets may allow a better understanding of fear and extinction memory processes.

Here I started to address the following questions: 1) To which intra- and extraamgygdaloid regions do mpITCs project in adult mice? 2) How is the communication infrastructure of mpITCs organized? 3) Which putative postsynaptic partners are targeted by mpITC axons?

I addressed these questions using fluorescent and confocal imaging, and axonal reconstruction of labeled mpITCs in brain slices. I obtained qualitative data that show mpITC axonal projection patterns in accordance with published cell types in juvenile animals. I also observed putative new intra-amygdala projection patterns to the basolateral complex and extra-amygdala projections to the caudate putamen and along amygdalo-striatal transition zone (Astr) to the internal capsule. In a subset of cells, we obtained 3D-reconstructions of axons using the Neurolucida software and determined quantitative parameters such as axonal length, branchpoints, and the number of presynaptic terminal boutons in specific target regions. Among these, axonal length in a specific region seems to be a main parameter that determines innervation efficacy. Lastly, I used confocal microscopy and immunohistochemical staining for markers of distinct neuron types in CEA and the Astr, to identify possible contact sites with mpITCs axons. Our findings suggest that mpITCs could make contacts with $Fear_{ON}$cells (SOM^{+}cells) and $Fear_{OFF}$cells (PKC δ $^{+}$cells) in CEA, but appear to pass cholinergic cells in the Astria.

Together, our results reveal an unprecedented complexity of axonal projection patterns and give first quantitative insights into the wiring and postsynaptic partners of mpITCs in adult

animals.

Zusammenfassung

Die Amygdala spielt eine zentrale Rolle in der Verarbeitung von Emotionen wie Angst und Furcht und darauf basierenden Erkrankungen. Sie befindet sich beidseits im Temporallappen und kann in weitere Subnuclei unterteilt werden. Sie wird von sensorischen Afferenzen innerviert und projiziert weiter zu kaudal liegenden Regionen, die verantwortlich für die Generierung u.a. von Angstverhalten sind. Während die Rolle glutamaterger Projektionsneuronen in der Amygdala bisher im Fokus lag, ist das Verständnis GABAerger Systeme bisher noch unzureichend. GABAerge Neuronen der Amygdala können durch Inhibition und Disinhibition modulierend in die Verarbeitung von Angst und Furcht eingreifen. Teil des inhibitorischen Netzwerks sind die sogenannten interkalierten Zellen (ITCs), die entlang der Faserbündel um den basolateralen Komplex (BLA) in Clustern angeordnet sind. Ergebnisse der letzten Jahre legen nahe, dass medial-parakapsuläre ITCs (mpITCs) an der Verarbeitung von erlernter Angst beteiligt sind, da sie sowohl während Angstkonditionierung, als auch Extinktionslernens aktiv sind und ihre Läsion das Extinktionsgedächtnis beeinträchtigt. Weiterhin zeigen diese Zellen ein heterogenes Projektionsmuster in jungen Mäusen. Daher gehen wir davon aus, dass die Untersuchung des efferenten Projektionsmusters und die Identifizierung postsynaptischer Partnerneurone in erwachsenen Mäusen zu einem besseren Verständnis des Angst- und Extinktionsgedächtnisses beiträgt.

Daraus ergeben sich folgende Fragen: 1) Zu welchen intra- und extraamygdaloiden Regionen projizieren mpITCs in erwachsenen Mäusen? 2) Ist eine gewisse Spezialisierung ihrer axonalen Kommunikationsinfrastruktur identifizierbar? 3) Mit welchen Zelltypen in den identifizierten Zielregionen gehen mpITCs mögliche Synapsen ein?

Zur Beantwortung dieser Fragen verwenden wir Fluoreszenz- und Konfokalmikroskopie und Rekonstruktion von mpITCs in koronaren Hirnschnitten. Qualitative Ergebnisse zeigen, dass sich das in jungen Tieren bekannte heterogene Projektionsmuster bestätigt und erweitert. Es zeigen sich auch bisher nicht bekannte Projektionsmuster: intraamygdaloid zum basolateralen Komplex, sowie extraamygdaloid zum Putamen und Nucleus caudatus und entlang der amygdalo-striatalen Übergangszone (Astr) zur Capsula interna. Einige Zellen wurden mit Neurolucida 3D-rekonstruiert und funktionell wichtige Parameter der axonalen Kommunikationsinfrastruktur wie Verzweigungsdichte, Varikositätendichte und Länge bestimmt. Dabei konnte Axonlänge als funktionell bedeutendster Parameter identifiziert werden. Es zeigten sich unter den mpITCs verschiedene Projektionstypen, die sich durch bevorzugt angesteuerte Zielregionen unterscheiden. Um Partnerzellen der mpITCs in den vorher eruierten Zielregionen auszumachen, wurden mit dem Konfokalmikroskop Bereiche untersucht, in denen sich

fluoreszenzgefärbte mpITC Axone an immunohistochemisch markierte Zelltypen der Zielregionen annähern. Hier erhielt ich erste Hinweise darauf, dass mpITCs an einflussreichen Stellen Angst verstärkender Zellen (SOM^+Zellen), als auch Angst vermindernder Zellen (PKC δ^+Zellen) mögliche Synapsen ausbilden. An cholinergen Neuronen ziehen mpITC Axone sehr nahe vorbei, jedoch ohne dort präsynaptische Köpfchen zu bilden.

Insgesamt zeigen meine Ergebnisse potentielle neue axonale Projektionsmuster der mpITCs und geben erste Hinweise auf eine gewisse Spezialisierung unter den mpITCs aufgrund bevorzugter Zielregionen und der beteiligten sich funktionell unterscheidenden postsynaptischen Partnerzellen.

6 Literature

References

Adolphs, R. (2013). The biology of fear. *Current biology: CB*, 23(2), R79–93.

Amano, T., Unal, C. T., & Paré, D. (2010). Synaptic correlates of fear extinction in the amygdala. *Nature Neuroscience*, 13(4), 489–494.

Amir, A., Amano, T., & Pare, D. (2011). Physiological identification and infralimbic responsiveness of rat intercalated amygdala neurons. *Journal of Neurophysiology*, 105(6), 3054–3066.

Asede, D., Bosch, D., Lüthi, A., Ferraguti, F., & Ehrlich, I. (2015). Sensory inputs to intercalated cells provide fear-learning modulated inhibition to the basolateral amygdala. *Neuron*, 86(2), 541–554.

Bear F. Mark, Connors W. Barry, & Paradiso A. Michael (2008). *Neurowissenschaften - ein grundlegendes Lehrbuch für Biologie, Medizin und Psychologie*. Springer Verlag, 3. deutsche Auflage, 44 - 45.

Berretta, S. (2005). Cortico-amygdala circuits: role in the conditioned stress response. *Stress (Amsterdam, Netherlands)*, 8(4), 221–232.

Bienvenu, T. C. M., Busti, D., Magill, P. J., Ferraguti, F., & Capogna, M. (2012). Cell-type-specific recruitment of amygdala interneurons to hippocampal theta rhythm and noxious stimuli inăvivo. *Neuron*, 74(6), 1059–1074.

Bienvenu, T. C. M., Busti, D., Micklem, B. R., Mansouri, M., Magill, P. J., Ferraguti, F., & Capogna, M. (2015). Large intercalated neurons of amygdala relay noxious sensory information. *The Journal of Neuroscience: The Official Journal of the Society for Neuroscience*, 35(5), 2044–2057.

Blaesse, P., Goedecke, L., Bazelot, M., Capogna, M., Pape, H.-C., & Jüngling, K. (2015). -Opioid Receptor-Mediated Inhibition of Intercalated Neurons and Effect on Synaptic Transmission to the Central Amygdala. *The Journal of Neuroscience: The Official Journal of the Society for Neuroscience*, 35(19), 7317–7325.

Bolam, J. P., Hanley, J. J., Booth, P. A., & Bevan, M. D. (2000). Synaptic organisation of the basal ganglia. *Journal of Anatomy*, 196 (Pt 4), 527–542.

Busti, D. (2012). *Morphological and functional characterization of inhibitory networks of the amygdala, Innsbruck University*. PhD thesis.

Busti, D., Geracitano, R., Whittle, N., Dalezios, Y., Mańko, M., Kaufmann, W., Sätzler, K., Singewald, N., Capogna, M., & Ferraguti, F. (2011). Different fear states engage distinct networks within the intercalated cell clusters of the amygdala. *The Journal of Neuroscience: The Official Journal of the Society for Neuroscience*, 31(13), 5131–5144.

Canty, A. & Murphy, M. (2008). Molecular mechanisms of axon guidance in the developing corticospinal tract. *Progress in Neurobiology*, 85(2), 214–235.

Cassell, M. D., Freedman, L. J., & Shi, C. (1999). The intrinsic organization of the central extended amygdala. *Annals of the New York Academy of Sciences*, 877, 217–241.

Chatelet Noelle (2000). *Das Sonnenblumenmädchen*. Verlag Kiepenheuer und Witsch, aus dem Französischen von Uli Wittmann, Titel der Orignialausgabe: "La petite aux tournesols", 1999, 110.

Cho, J.-H., Deisseroth, K., & Bolshakov, V. Y. (2013). Synaptic encoding of fear extinction in mPFC-amygdala circuits. *Neuron*, 80(6), 1491–1507.

Ciocchi, S., Herry, C., Grenier, F., Wolff, S. B. E., Letzkus, J. J., Vlachos, I., Ehrlich, I., Sprengel, R., Deisseroth, K., Stadler, M. B., Müller, C., & Lüthi, A. (2010). Encoding of conditioned fear in central amygdala inhibitory circuits. *Nature*, 468(7321), 277–282.

Cocas, L. A., Miyoshi, G., Carney, R. S. E., Sousa, V. H., Hirata, T., Jones, K. R., Fishell, G., Huntsman, M. M., & Corbin, J. G. (2009). Emx1-lineage progenitors differentially contribute to neural diversity in the striatum and amygdala. *The Journal of Neuroscience: The Official Journal of the Society for Neuroscience*, 29(50), 15933–15946.

Davis, M. & Shi, C. (1999). The extended amygdala: are the central nucleus of the amygdala and the bed nucleus of the stria terminalis differentially involved in fear versus anxiety? *Annals of the New York Academy of Sciences*, 877, 281–291.

Davis, M., Walker, D. L., Miles, L., & Grillon, C. (2010). Phasic vs sustained fear in rats and humans: role of the extended amygdala in fear vs anxiety. *Neuropsychopharmacol-*

ogy: Official Publication of the American College of Neuropsychopharmacology, 35(1), 105–135.

Davis, n. & Shi, n. (2000). The amygdala. *Current biology: CB*, 10(4), R131.

Dobi, A., Sartori, S. B., Busti, D., Van der Putten, H., Singewald, N., Shigemoto, R., & Ferraguti, F. (2013). Neural substrates for the distinct effects of presynaptic group III metabotropic glutamate receptors on extinction of contextual fear conditioning in mice. *Neuropharmacology*, 66, 274–289.

Duvarci, S. & Pare, D. (2014). Amygdala microcircuits controlling learned fear. *Neuron*, 82(5), 966–980.

Franklin, K. B. & George Paxinos (2008). *The Mouse Brain in Stereotaxic Coordinates*. Academic Press, 3rd illustrated edition.

Geracitano, R., Kaufmann, W. A., Szabo, G., Ferraguti, F., & Capogna, M. (2007). Synaptic heterogeneity between mouse paracapsular intercalated neurons of the amygdala. *The Journal of Physiology*, 585(Pt 1), 117–134.

Haubensak, W., Kunwar, P. S., Cai, H., Ciocchi, S., Wall, N. R., Ponnusamy, R., Biag, J., Dong, H.-W., Deisseroth, K., Callaway, E. M., Fanselow, M. S., Lüthi, A., & Anderson, D. J. (2010). Genetic dissection of an amygdala microcircuit that gates conditioned fear. *Nature*, 468(7321), 270–276.

Hefner, K., Whittle, N., Juhasz, J., Norcross, M., Karlsson, R.-M., Saksida, L. M., Bussey, T. J., Singewald, N., & Holmes, A. (2008). Impaired fear extinction learning and cortico-amygdala circuit abnormalities in a common genetic mouse strain. *The Journal of Neuroscience: The Official Journal of the Society for Neuroscience*, 28(32), 8074–8085.

Herry, C., Ciocchi, S., Senn, V., Demmou, L., Müller, C., & Lüthi, A. (2008). Switching on and off fear by distinct neuronal circuits. *Nature*, 454(7204), 600–606.

Huang, C.-C., Chen, C.-C., Liang, Y.-C., & Hsu, K.-S. (2014). Long-term potentiation at excitatory synaptic inputs to the intercalated cell masses of the amygdala. *The International Journal of Neuropsychopharmacology*, 17(8), 1233–1242.

Jacobsen, K. X., Höistad, M., Staines, W. A., & Fuxe, K. (2006). The distribution of dopamine D1 receptor and mu-opioid receptor 1 receptor immunoreactivities in the amyg-

dala and interstitial nucleus of the posterior limb of the anterior commissure: relationships to tyrosine hydroxylase and opioid peptide terminal systems. *Neuroscience*, 141(4), 2007–2018.

Janak, P. H. & Tye, K. M. (2015). From circuits to behaviour in the amygdala. *Nature*, 517(7534), 284–292.

Jüngling, K., Seidenbecher, T., Sosulina, L., Lesting, J., Sangha, S., Clark, S. D., Okamura, N., Duangdao, D. M., Xu, Y.-L., Reinscheid, R. K., & Pape, H.-C. (2008). Neuropeptide S-mediated control of fear expression and extinction: role of intercalated GABAergic neurons in the amygdala. *Neuron*, 59(2), 298–310.

Jolkkonen, E., Miettinen, R., Pikkarainen, M., & Pitkänen, A. (2002). Projections from the amygdaloid complex to the magnocellular cholinergic basal forebrain in rat. *Neuroscience*, 111(1), 133–149.

Jovanovic, T. & Norrholm, S. D. (2011). Neural mechanisms of impaired fear inhibition in posttraumatic stress disorder. *Frontiers in Behavioral Neuroscience*, 5, 44.

Keane, T. M., Marshall, A. D., & Taft, C. T. (2006). Posttraumatic stress disorder: etiology, epidemiology, and treatment outcome. *Annual Review of Clinical Psychology*, 2, 161–197.

Keshavarzi, S., Sullivan, R. K. P., Ianno, D. J., & Sah, P. (2014). Functional properties and projections of neurons in the medial amygdala. *The Journal of Neuroscience: The Official Journal of the Society for Neuroscience*, 34(26), 8699–8715.

Kirkegaard Sören (1992). *Der Begriff Angst*. Reclam Verlag, aus dem Dänischen von Gisela Perlet, Titel der Originalausgabe: Begrebet Angest, 1844, 53.

Knapska, E. & Maren, S. (2009). Reciprocal patterns of c-Fos expression in the medial prefrontal cortex and amygdala after extinction and renewal of conditioned fear. *Learning & Memory (Cold Spring Harbor, N.Y.)*, 16(8), 486–493.

Krémarik, P., Freund-Mercier, M. J., & Pittman, Q. J. (1995). Fundus striati vasopressin receptors in blood pressure control. *The American Journal of Physiology*, 269(3 Pt 2), R497–503.

LeDoux, J. (2007). The amygdala. *Current biology: CB*, 17(20), R868–874.

LeDoux, J. E. (2000). Emotion circuits in the brain. *Annual Review of Neuroscience*, 23, 155–184.

LeDoux, J. E., Iwata, J., Cicchetti, P., & Reis, D. J. (1988). Different projections of the central amygdaloid nucleus mediate autonomic and behavioral correlates of conditioned fear. *The Journal of Neuroscience: The Official Journal of the Society for Neuroscience*, 8(7), 2517–2529.

Leyva-Díaz, E. & López-Bendito, G. (2013). In and out from the cortex: development of major forebrain connections. *Neuroscience*, 254, 26–44.

Li, H., Penzo, M. A., Taniguchi, H., Kopec, C. D., Huang, Z. J., & Li, B. (2013). Experience-dependent modification of a central amygdala fear circuit. *Nature Neuroscience*, 16(3), 332–339.

Likhtik, E., Popa, D., Apergis-Schoute, J., Fidacaro, G. A., & Paré, D. (2008). Amygdala intercalated neurons are required for expression of fear extinction. *Nature*, 454(7204), 642–645.

Mańko, M., Geracitano, R., & Capogna, M. (2011). Functional connectivity of the main intercalated nucleus of the mouse amygdala. *The Journal of Physiology*, 589(Pt 8), 1911–1925.

Maren, S. (2001). Neurobiology of Pavlovian fear conditioning. *Annual Review of Neuroscience*, 24, 897–931.

Maren, S. (2003). The amygdala, synaptic plasticity, and fear memory. *Annals of the New York Academy of Sciences*, 985, 106–113.

Marowsky, A., Yanagawa, Y., Obata, K., & Vogt, K. E. (2005). A specialized subclass of interneurons mediates dopaminergic facilitation of amygdala function. *Neuron*, 48(6), 1025–1037.

McDonald, A. J. (1992). Projection neurons of the basolateral amygdala: a correlative Golgi and retrograde tract tracing study. *Brain Research Bulletin*, 28(2), 179–185.

McDonald, A. J., Mascagni, F., & Guo, L. (1996). Projections of the medial and lateral prefrontal cortices to the amygdala: a Phaseolus vulgaris leucoagglutinin study in the rat. *Neuroscience*, 71(1), 55–75.

Milad, M. R., Furtak, S. C., Greenberg, J. L., Keshaviah, A., Im, J. J., Falkenstein, M. J., Jenike, M., Rauch, S. L., & Wilhelm, S. (2013). Deficits in conditioned fear extinction in obsessive-compulsive disorder and neurobiological changes in the fear circuit. *JAMA psychiatry*, 70(6), 608–618; quiz 554.

Millhouse, O. E. (1986). The intercalated cells of the amygdala. *The Journal of Comparative Neurology*, 247(2), 246–271.

Palomares-Castillo, E., Hernández-Pérez, O. R., Pérez-Carrera, D., Crespo-Ramírez, M., Fuxe, K., & Pérez de la Mora, M. (2012). The intercalated paracapsular islands as a module for integration of signals regulating anxiety in the amygdala. *Brain Research*, 1476, 211–234.

Pape, H.-C. & Pare, D. (2010). Plastic synaptic networks of the amygdala for the acquisition, expression, and extinction of conditioned fear. *Physiological Reviews*, 90(2), 419–463.

Paré, D., Quirk, G. J., & Ledoux, J. E. (2004). New vistas on amygdala networks in conditioned fear. *Journal of Neurophysiology*, 92(1), 1–9.

Penzo, M. A., Robert, V., & Li, B. (2014). Fear conditioning potentiates synaptic transmission onto long-range projection neurons in the lateral subdivision of central amygdala. *The Journal of Neuroscience: The Official Journal of the Society for Neuroscience*, 34(7), 2432–2437.

Penzo, M. A., Robert, V., Tucciarone, J., De Bundel, D., Wang, M., Van Aelst, L., Darvas, M., Parada, L. F., Palmiter, R. D., He, M., Huang, Z. J., & Li, B. (2015). The paraventricular thalamus controls a central amygdala fear circuit. *Nature*, 519(7544), 455–459.

Phelps, E. A. & LeDoux, J. E. (2005). Contributions of the amygdala to emotion processing: from animal models to human behavior. *Neuron*, 48(2), 175–187.

Pinard, C. R., Mascagni, F., & McDonald, A. J. (2012). Medial prefrontal cortical innervation of the intercalated nuclear region of the amygdala. *Neuroscience*, 205, 112–124.

Pinto, A. & Sesack, S. R. (2008). Ultrastructural analysis of prefrontal cortical inputs to the rat amygdala: spatial relationships to presumed dopamine axons and D1 and D2 receptors. *Brain Structure & Function*, 213(1-2), 159–175.

Pitkänen, A., Savander, V., & LeDoux, J. E. (1997). Organization of intra-amygdaloid circuitries in the rat: an emerging framework for understanding functions of the amygdala. *Trends in Neurosciences*, 20(11), 517–523.

Price, J. L. (2003). Comparative aspects of amygdala connectivity. *Annals of the New York Academy of Sciences*, 985, 50–58.

Royer, S., Martina, M., & Paré, D. (1999). An inhibitory interface gates impulse traffic between the input and output stations of the amygdala. *The Journal of Neuroscience: The Official Journal of the Society for Neuroscience*, 19(23), 10575–10583.

Sah, P., Faber, E. S. L., Lopez De Armentia, M., & Power, J. (2003). The amygdaloid complex: anatomy and physiology. *Physiological Reviews*, 83(3), 803–834.

Scibilia, R. J., Lachowicz, J. E., & Kilts, C. D. (1992). Topographic nonoverlapping distribution of D1 and D2 dopamine receptors in the amygdaloid nuclear complex of the rat brain. *Synapse (New York, N.Y.)*, 11(2), 146–154.

Senn, V., Wolff, S. B. E., Herry, C., Grenier, F., Ehrlich, I., Gründemann, J., Fadok, J. P., Müller, C., Letzkus, J. J., & Lüthi, A. (2014). Long-range connectivity defines behavioral specificity of amygdala neurons. *Neuron*, 81(2), 428–437.

Shammah-Lagnado, S. J., Alheid, G. F., & Heimer, L. (1996). Efferent connections of the caudal part of the globus pallidus in the rat. *The Journal of Comparative Neurology*, 376(3), 489–507.

Shammah-Lagnado, S. J., Alheid, G. F., & Heimer, L. (1999). Afferent connections of the interstitial nucleus of the posterior limb of the anterior commissure and adjacent amygdalostriatal transition area in the rat. *Neuroscience*, 94(4), 1097–1123.

Shammah-Lagnado, S. J., Alheid, G. F., & Heimer, L. (2001). Striatal and central extended amygdala parts of the interstitial nucleus of the posterior limb of the anterior commissure: evidence from tract-tracing techniques in the rat. *The Journal of Comparative Neurology*, 439(1), 104–126.

Sigurdsson, T., Doyère, V., Cain, C. K., & LeDoux, J. E. (2007). Long-term potentiation in the amygdala: a cellular mechanism of fear learning and memory. *Neuropharmacology*, 52(1), 215–227.

Strobel, C., Marek, R., Gooch, H. M., Sullivan, R. K. P., & Sah, P. (2015). Prefrontal and Auditory Input to Intercalated Neurons of the Amygdala. *Cell Reports*.

Tepper, J. M. & Bolam, J. P. (2004). Functional diversity and specificity of neostriatal interneurons. *Current Opinion in Neurobiology*, 14(6), 685–692.

Trepel Martin (2008). *Neuroanatomie - Struktur und Funktion*. Urban und Fischer Verlag, 4. Auflage, 4.

Waclaw, R. R., Ehrman, L. A., Pierani, A., & Campbell, K. (2010). Developmental origin of the neuronal subtypes that comprise the amygdalar fear circuit in the mouse. *The Journal of Neuroscience: The Official Journal of the Society for Neuroscience*, 30(20), 6944–6953.

Weiskrantz, L. (1956). Behavioral changes associated with ablation of the amygdaloid complex in monkeys. *Journal of Comparative and Physiological Psychology*, 49(4), 381–391.

Whittle, N., Hauschild, M., Lubec, G., Holmes, A., & Singewald, N. (2010). Rescue of impaired fear extinction and normalization of cortico-amygdala circuit dysfunction in a genetic mouse model by dietary zinc restriction. *The Journal of Neuroscience: The Official Journal of the Society for Neuroscience*, 30(41), 13586–13596.

Wilensky, A. E., Schafe, G. E., Kristensen, M. P., & LeDoux, J. E. (2006). Rethinking the fear circuit: the central nucleus of the amygdala is required for the acquisition, consolidation, and expression of Pavlovian fear conditioning. *The Journal of Neuroscience: The Official Journal of the Society for Neuroscience*, 26(48), 12387–12396.

List of Figures

7 Declaration of the proportion of own work

The concept of the study was done by my supervisor Dr. Ingrid Ehrlich, in collaboration with Dr. Douglas Asede, former PhD student in the lab, and me. For this project, I obtained mpITCs that had been filled by Dr. Douglas Asede during recording. All experiments on this material, unless explicitly mentioned otherwise below, were performed by me.

For Results part 3.1, I performed resectioning and staining of 19 cells with streptavidin-conjugated fluorophores to reveal axonal identity. Altogether, I documented a total of 93 cells, some of which were previously sectioned and stained. Out of these 93 cells, 39 cells fit the criteria to be analyzed and they were characterized fully by me and named the "small dataset" in part 3.1. The other cells shown in the "large dataset" for comparison were sectioned, processed and analyzed by Douglas Asede and Minas Salib in the Ehrlich lab.

For Results part 3.2, successful DAB-conversion of 7 mpITCs was performed by me, as well as the complete Neurolucida reconstruction of 8 cells, and the subsequent quantification of a total of 10 cells (Part 3.2). Michaela Richter, a former intern in the lab that I co-supervised, helped with the reconstruction and quantification of 2 cells. The statistical analysis was done by me.

For Results part 3.3, all immunohistochemical stainings and the entire confocal analysis were performed by me.

I ensure that the entire thesis was written by me with formatting advice by the IZKF-Promotionskolleg and under the supervision of Dr. Ingrid Ehrlich. I did not use any further references than the ones stated in the text.

Tübingen,

Acknowledgments

I wish to thank my supervisor Dr. Ingrid Ehrlich for her support and guidance in this medical doctoral thesis project. Also, I wish to express my thanks to my Co-Supervisor, Dr. Douglas Asede for his encouraging way of working together as well as all other members of the Ehrlich laboratory for their supporting attitude and friendship. Special thanks to the head of a collaborating laboratory Prof. Dr Ferraguti and one of his technical assistants, Gabi Schmid, for her introduction to Neurolucida. I would like to show my acknowledgments to Prof. Dr. Marlies Knipper and the team of the IZKF-Promotionskolleg for their guidance throughout this thesis process.

Also, I wish to thank my parents for their critical opinion and loving support. Thanks to Philipp, for his opinion that dedication to work is something good, to Sophia, for her writing company, to Christoph for his introduction to Lyx, to Reinhardt for the two sided caption, and to the members of the Leibnizhaus for the refreshing different atmosphere after lab days.